1982).

The analysis of hepatotoxicity of MP has been repeatedly performed by various techniques including the toxicogenomics approach (Hamadeh *et al.*, 2002). This compound induces marked and reproducible hepatic injury in rodents, and was used to assess the validity of toxicogenomics analyses among the multicenter platform (Waring *et al.*, 2004; Chu *et al.*, 2004). In the former study, there was a pessimistic interpretation that microarrays never supply highly reliable measures because of too large variance between research facilities. In this case, samples from the same animal were analyzed in multiple facilities but there were almost no genes that were detected as commonly changed in all the facilities. However, the latter study revealed that the robustness of the results regarding the movement of certain toxicological pathways was sufficient although the fitness of each gene was somewhat questionable. In other words, when we have a reasonable list of genes with certain toxicological significance, the reliability would be highly improved. The strategy of our project follows this idea, i.e., the results are interpreted as a trend for a set of functional genes.

Presently extracted genes from the group receiving the highest dose (showing obvious phenotypes) were categorized and this revealed that genes related to the regulation of cell cycle, MAPK signaling, and the glutathione metabolism were all involved in the development of the presently observed phenotypes. As for the down-regulated genes in repeated dosing, it could be a reflection of the failure of hepatic functions, *i.e.*, metabolism of sugar and sterols, and production of functional proteins such as complements and blood coagulation.

To facilitate the analytical procedures for our large-scale microarray database, we developed two types of the one-dimensional score, named as TGP1 and TGP2, which express the trend of the changes in expression of biomarker genes as a whole. The former is based on the signal log ratio (Kiyosawa *et al.*, 2006) and is convenient to compare the responsiveness of many drugs to a marker gene list. The disadvantages of this scoring system are that it overestimates the responsiveness when the list contains a gene where the induction is extreme (such as CYP1A1) and it

Table 5. Time course changes of TGP-1 scores in selected MP-responsive gene lists.

MP-RESPONSIVE GENE LISTS	03H			06H			09H			24H		
	L	M	H	L	M	H	L	M	H	L	M	H
GLUTATHIONE METABOLISM	23	2	7	2	39	607	−2	24	498	−35	−1	409
APOPTOSIS	6	7	103	3	24	342	8	10	128	0	2	195
MAPK SIGNALING PATHWAY	3	9	190	−2	7	114	−5	−26	15	−5	−2	57
REGULATION OF CELL CYCLE	3	2	108	−2	5	133	−3	−1	33	−3	−2	21
MP-RESPONSIVE GENE LISTS	04D			08D			15D			29D		
	L	M	H	L	M	H	L	M	H	L	M	H
GLUTATHIONE METABOLISM	2	118	476	2	170	3466	0	235	2285	5	712	2865
APOPTOSIS	2	54	286	93	227	1172	3	154	1360	−4	115	1396
MAPK SIGNALING PATHWAY	13	3	34	13	60	295	3	68	354	7	29	378
REGULATION OF CELL CYCLE	10	4	7	13	20	219	1	15	247	4	28	470

AFFYMETRIX PROBE ID	SYMBOL	03H			06H			09H			24H			04D			08D			15D			29D		
		L	M	H	L	M	H	L	M	H	L	M	H	L	M	H	L	M	H	L	M	H	L	M	H
1367858_at	G6pdx	1.1	0.9	0.9	1.2	1.4	2.5	1.1	1.5	4.2	1.0	1.4	2.9	1.4	0.8	1.4	0.6	0.9	1.8	1.1	1.2	3.9	1.0	0.8	5.0
1368374_a_at	Ggt1	1.1	1.0	0.9	1.1	0.9	0.7	1.0	0.7	0.9	1.0	1.2	1.3	1.0	1.0	1.3	1.3	1.4	2.8	1.1	1.3	4.5	0.9	1.3	8.0
1369061_at	Gsr	1.2	1.1	1.2	1.1	1.5	1.8	1.2	1.8	2.7	0.9	1.2	1.7	0.9	1.2	1.2	1.0	1.2	2.1	0.8	1.0	1.6	0.9	1.2	1.9
1369921_at	Gstm4	1.1	1.1	1.1	1.2	2.0	12	0.7	1.1	6.9	0.4	0.7	6.6	1.2	4.6	7.7	1.1	1.0	63	0.7	5.0	30	1.3	8.8	8.5
1369926_at	Gpx3	1.1	1.0	0.9	1.2	1.0	1.1	0.8	0.9	0.8	0.9	0.9	0.9	1.0	1.0	0.8	0.9	0.9	2.0	1.0	1.1	2.9	1.1	1.3	9.1
1370030_at	Gclm	1.1	1.2	1.3	1.2	1.4	2.5	1.2	1.8	2.1	0.9	0.7	1.0	1.1	1.3	1.0	1.1	1.0	1.6	1.0	1.2	1.3	0.9	0.8	1.0
1370365_at	Gss	1.4	1.1	1.2	1.0	1.3	1.2	0.9	1.0	1.2	1.1	1.1	2.1	0.9	1.1	1.6	0.7	0.9	2.0	1.0	1.1	2.7	1.0	1.2	2.4
1371089_at	Yc2	2.4	1.3	1.4	1.0	1.8	2.8	0.9	1.4	3.9	0.7	1.2	5.6	0.9	1.9	6.7	1.7	5.9	30	1.4	4.6	20	1.7	11	34
1372623_at	Gclc	1.4	1.4	1.7	1.4	2.4	3.6	1.4	2.2	3.8	1.0	0.9	1.4	0.9	1.2	1.3	1.0	1.1	1.1	1.0	1.1	1.0	0.9	1.0	1.0
1374070_at	Gpx2	1.3	0.9	1.0	1.2	1.0	1.8	0.7	0.6	1.5	0.9	1.0	1.3	1.4	1.2	2.0	1.4	1.1	3.7	1.2	1.3	3.4	1.3	1.6	13

The number in each column expresses the ratio to control (N=3).

Fig. 3. Heatmap of individual gene expression change in category of "glutathione metabolism".

also underestimates the responsiveness when the genes in the list are mobilized to either direction. To overcome these disadvantages, we employed another score, TGP2, based on the effect size. In the present study, we employed the TGP1 score for assessment of the responsiveness to the gene lists, *i.e.*, "regulation of cell cycle", "MAPK signaling" and "glutathione metabolism" since the direction of expression changes was uniform. In the highest dose group, the scores for these categories markedly increased from the early time point after single dose and kept their high expression throughout the repeated dose period. In the middle dose groups, the increment of the scores were noted not only at the time points when apparent pathological changes emerged, but also at the earlier stage of repeated dosing and even after single dosing. This indicates that the toxicogenomics approach enables more sensitive assessment at the earlier time point than classical toxicology evaluation. Among the responding genes, glutathione-related: glucose-6-phosphate dehydrogenase (G6pdx), glutathione *S*-transferase M4 (Gstm4) and glutathione *S*-transferase Yc2 subunit (Yc2), apoptosis related: nucleolar protein 3 (Nol3), rhoB gene (Rhob) and tribbles homolog 3 (Drosophila) (Trib3), MAPK signaling-related: myelocytomatosis viral oncogene homolog (avian) (Myc), FBJ murine osteosarcoma viral oncogene homolog (Fos), v-jun sarcoma virus 17 oncogene homolog (avian) (Jun) and fibroblast growth factor 21 (Fgf21), and DNA damage-related: growth arrest and DNA-damage-inducible 45 alpha (Gadd45a) and DNA-damage inducible transcript 3 (Ddit3), these were markedly up-regulated from the early point of dosing. Especially, Trib3, which showed typical changes in the present study, would be one

AFFYMETRIX PROBE ID	SYMBOL	03H			06H			09H			24H			04D			08D			15D			29D		
		L	M	H	L	M	H	L	M	H	L	M	H	L	M	H	L	M	H	L	M	H	L	M	H
1367827_at	Ppp2cb	1.1	1.0	1.0	0.9	0.9	1.0	1.1	1.0	1.0	0.9	0.9	1.1	0.9	1.0	1.1	1.0	1.1	1.8	0.9	1.2	2.1	1.0	1.2	2.2
1367831_at	Tp53	1.1	1.2	1.2	0.9	0.8	1.0	1.0	0.9	0.9	0.9	1.0	1.1	1.3	1.0	1.3	1.3	1.3	2.0	1.3	1.0	2.4	0.8	1.2	2.0
1367856_at	G6pdx	0.9	1.2	4.8	1.1	1.6	13	1.3	1.5	2.8	1.0	1.0	1.1	1.4	0.8	1.4	0.6	0.9	1.8	1.1	1.2	3.9	1.0	0.8	5.0
1367890_at	Casp2	1.0	0.8	0.8	1.0	0.8	0.9	0.9	1.1	0.8	0.9	1.0	1.1	1.1	1.0	1.0	1.1	1.2	1.3	0.9	1.0	1.2	1.1	1.1	1.9
1367922_at	Adam17	1.0	1.1	0.9	1.0	1.1	1.5	1.1	1.2	1.8	1.0	1.0	1.1	1.1	0.9	1.0	1.1	1.1	1.0	1.1	0.9	1.1	1.1	1.1	1.7
1368118_at	Bcl10	0.9	0.9	1.0	1.0	0.9	0.8	1.0	0.8	0.9	0.9	1.1	1.1	1.1	0.9	1.0	0.9	0.9	1.6	0.9	1.0	1.6	1.1	1.3	1.8
1368306_at	Casp6	1.1	1.0	1.0	0.7	0.9	0.8	0.8	0.8	0.9	0.9	0.9	1.0	1.3	1.0	1.4	1.0	0.9	1.1	1.0	1.1	1.1	0.9	1.1	1.8
1368544_a_at	Nol3	1.2	1.8	3.1	2.2	3.2	13	1.2	1.0	2.5	2.2	1.5	4.3	1.4	1.4	1.4	1.5	1.0	2.9	1.3	1.5	7.5	0.6	2.5	10
1368856_at	Jak2	1.1	1.1	1.0	1.1	0.9	1.1	1.0	1.1	1.1	1.3	1.2	1.3	1.3	1.0	1.1	1.0	1.1	1.6	1.0	0.8	2.4	0.9	1.1	3.0
1368882_at	Akt1	0.5	0.7	0.9	0.8	1.4	1.6	1.9	3.7	4.5	1.1	1.2	1.4	0.9	0.8	0.9	1.0	0.9	1.3	1.0	1.0	1.6	0.8	1.0	1.4
1368888_a_at	Rtn4	1.1	1.0	1.1	0.9	1.2	1.9	1.1	1.3	1.9	1.1	0.9	1.1	1.3	0.9	1.0	0.9	1.8	2.5	1.3	1.8	2.7	0.8	1.7	4.2
1369104_at	Prkaa1	1.2	1.3	1.8	0.9	1.3	2.6	1.4	1.2	1.3	1.0	0.7	1.0	0.9	1.1	1.3	0.7	0.8	1.6	0.9	1.4	2.1	1.0	1.5	2.0
1369122_at	Bax	1.1	1.1	1.1	0.9	1.1	1.1	1.0	0.9	1.1	1.0	1.0	1.2	1.0	0.9	1.2	1.2	1.4	3.7	0.8	1.1	3.3	0.8	1.6	4.3
1369948_at	Ngfrap1	1.0	1.0	1.0	1.0	1.0	1.0	1.0	0.9	1.3	0.9	1.0	1.4	1.3	1.7	1.7	0.7	1.1	12	1.5	1.7	37	0.9	4.5	53
1369968_at	Rhob	1.0	1.4	2.9	1.2	1.2	3.4	1.2	1.0	2.2	1.1	1.1	2.7	0.9	1.0	1.1	1.0	1.1	2.0	1.2	1.3	3.0	1.0	1.5	3.9
1369995_at	Faf1	0.9	0.9	0.9	1.0	1.0	1.0	1.0	1.1	1.1	1.1	0.9	1.1	1.0	1.0	1.0	1.0	1.0	1.3	0.9	0.9	1.2	1.0	1.0	1.6
1370080_at	Hmox1	0.8	0.9	1.0	1.0	1.0	1.2	1.0	0.8	0.8	1.1	0.8	1.3	1.2	1.0	1.0	1.1	1.1	1.7	1.2	1.4	2.1	0.9	1.1	2.5
1370113_at	Birc3	1.0	1.0	1.1	0.8	1.2	1.1	1.2	0.9	1.2	1.1	1.1	1.2	1.3	0.9	1.2	0.9	0.9	1.1	0.7	0.9	1.4	1.0	1.2	1.9
1370141_at	Mcl1	0.9	1.0	1.0	1.0	1.0	1.1	1.0	0.9	0.9	1.0	1.1	1.3	1.1	1.1	1.2	1.0	1.2	1.6	1.1	1.2	1.4	0.9	1.0	1.6
1370226_at	Cstb	0.9	1.0	1.7	1.0	1.0	3.9	1.2	1.1	1.9	0.8	0.7	0.9	1.2	1.0	1.1	0.9	1.2	1.4	1.0	1.2	2.0	1.0	1.1	2.4
1370243_a_at	Ptma	0.9	0.8	0.9	1.1	1.0	0.9	0.9	0.7	0.8	1.0	1.2	1.2	1.0	0.9	1.0	1.0	1.0	1.3	0.9	1.0	1.5	0.9	1.1	1.7
1370290_at	Tubb5	1.0	1.1	1.2	0.9	1.1	1.4	1.0	1.1	1.1	0.9	0.9	1.0	1.1	1.1	1.1	0.8	0.8	1.3	0.9	0.9	1.8	1.1	1.2	2.6
1370695_s_at	Trib3	0.9	1.1	0.9	1.2	1.5	3.7	1.1	1.3	3.1	1.3	1.5	1.9	1.0	6.5	27	9.8	21	137	1.1	13	77	2.6	8.0	40
1371672_at	App	1.1	0.9	0.9	1.2	1.4	2.5	1.1	1.5	4.2	1.0	1.4	2.9	1.1	1.0	1.4	1.1	1.4	5.0	1.1	1.7	8.0	1.0	2.3	8.9
1373733_at	Bok	0.9	0.9	0.9	0.9	1.0	1.1	1.1	1.2	1.2	0.9	1.0	1.4	1.2	1.0	1.1	1.2	1.0	1.1	1.0	1.0	2.2	1.0	1.1	3.5
1386866_at	Ywhag	1.1	1.0	1.1	1.0	1.0	1.1	1.1	1.0	1.1	1.0	1.0	1.2	1.0	1.0	1.2	1.1	1.2	1.7	1.0	1.1	1.8	1.0	1.2	2.2
1387021_at	Wig1	1.0	1.1	1.1	1.1	1.1	1.7	1.1	1.1	1.6	0.9	0.9	1.2	1.1	1.0	1.1	0.9	1.0	1.5	1.1	1.1	2.3	1.2	1.3	3.4
1387087_at	Cebpb	0.9	1.0	1.0	1.2	1.3	0.7	0.6	0.8	0.7	0.6	0.8	1.7	1.3	1.5	1.3	1.5	1.2	1.6	0.9	1.3	1.6	0.7	1.1	0.8
1387502_at	Stk17b	1.1	1.3	1.4	0.9	1.0	1.9	1.3	1.1	1.1	0.8	1.0	1.1	1.2	1.1	1.2	1.2	1.2	1.6	1.0	1.0	1.5	0.9	1.1	2.0
1387605_at	Casp12	1.0	1.1	1.0	0.9	1.0	1.4	1.1	0.9	1.2	0.9	0.6	1.0	1.3	1.0	1.6	1.2	1.1	1.7	1.8	2.6	5.3	0.4	0.9	1.6
1387818_at	Casp11	2.5	2.3	1.3	1.2	1.0	1.0	0.8	0.9	0.7	1.3	1.7	2.9	1.1	0.9	1.5	1.1	1.2	3.3	1.4	1.7	7.4	0.6	1.6	4.5
1388099_a_at	Tfpt	0.8	0.9	0.9	1.0	1.0	1.0	1.1	0.9	1.0	1.3	1.8	1.6	0.9	0.8	1.1	0.9	0.9	1.4	0.9	1.1	1.9	1.1	1.3	2.6
1388120_at	Pdcd8ip	0.7	2.9	8.0	0.9	3.9	14	2.7	2.9	8.5	1.4	0.6	16	1.0	1.0	1.2	0.9	1.0	1.3	1.0	1.0	1.5	0.9	1.0	1.6
1388674_at	Cdkn1a	1.0	1.1	1.0	0.9	1.0	1.0	0.9	1.0	1.5	1.0	1.3	2.0	1.1	1.0	1.5	0.9	1.5	2.1	1.2	1.8	2.1	0.8	1.9	1.7
1388805_at	Ppp2ca	0.9	0.8	0.9	0.9	1.0	1.1	0.9	0.9	1.1	0.9	1.1	1.1	1.2	1.1	1.5	0.9	1.0	1.7	0.8	1.0	2.7	1.1	1.3	3.6
1388867_at	MGC112830	0.9	1.1	1.2	1.2	1.3	1.7	1.0	1.2	1.6	0.8	0.8	1.0	1.0	1.1	1.1	0.9	1.1	1.3	1.0	1.0	1.2	0.9	1.0	1.7
1389170_at	Casp7	1.0	1.1	1.2	0.9	1.0	0.9	1.0	0.8	1.1	1.3	1.0	1.0	1.0	1.0	1.1	1.0	1.1	1.3	1.0	1.0	1.5	1.1	1.2	1.8
1398948_at	Tax1bp1	0.8	0.8	0.8	1.2	1.0	0.9	1.3	1.0	1.3	1.3	1.8	2.1	1.0	1.1	1.2	1.1	1.2	1.5	1.0	1.1	1.5	1.1	1.1	1.7

The number in each column expresses the ratio to control (N=3).

Fig. 4. Heatmap of individual gene expression change in category of "apoptosis".

of the promising candidates of biomarker genes for oxidative stress-mediated DNA damage, since it was reported to be up-regulated specifically by stress-inducing DNA damage (Corcoran *et al.*, 2005).

It was reported that hepatotoxicity of MP was due to its active metabolite(s) and that oxidative stress was involved (Ratra *et al.*, 1998). However, these authors excluded the involvement of glutathione depletion followed by oxidative stress in the later paper (Ratra *et al.*, 2000). We measured hepatic glutathione contents in rats treated with MP in a separate study (Uehara *et al.*, submitted). Immediately after MP dosing, a transient decrease, not statistically significant, was noted and a rebound-like increase was evident at 24 hr after dosing, which persisted for one week. The increment of glutathione contents disappeared till 2 weeks and it turned to a marked decrease after 4 weeks. These results suggest that MP causes oxidative stress in consuming glutathione while the hepatocytes defend against it by gene expression changes to keep a high glutathione level. Finally, glutathione depletion occurs when the toxicity of MP persists for a long period. We have extracted marker genes for hepatic glutathione depletion using a glutathione depletor, phorone (Kiyosawa *et al.*, 2007). Also in this work, phorone caused a transient decrease of glutathione with a peak at 3 to 6 hr after dosing followed by a rebound-like increase 24 hr after dosing. Taken together, the key of hepatotoxicity of MP is considered to be oxidative damage of DNA followed by changes in MAPK signaling and cell cycle induced by excess production of active metabolites. Sustained oxidative damage of DNA and stimulation of cell proliferation is closely related to hepatocarcinogenesis of MP.

The main purpose of the toxicogenomics approach was to analyze the mechanism of toxicity and predict chronic toxicity from acute data in the preclinical study. In the present study, we simulated the prediction of the toxicity

AFFYMETRIX	SYMBOL	03H			06H			09H			24H			04D			08D			15D			29D		
PROBE ID		L	M	H	L	M	H	L	M	H	L	M	H	L	M	H	L	M	H	L	M	H	L	M	H
1367577_at	Hspb1	1.0	0.9	0.6	1.3	1.4	1.4	0.6	0.8	1.0	1.2	1.3	2.0	1.2	1.5	1.1	1.4	1.3	2.9	0.9	1.3	3.1	0.9	1.6	2.9
1367624_at	Atf4	1.0	1.2	1.8	0.9	1.3	2.2	1.5	1.4	2.2	1.0	0.9	1.3	1.1	1.1	1.3	1.2	1.2	1.6	0.9	1.1	2.0	1.1	1.0	2.0
1367760_at	Map2k1	1.0	1.1	1.1	1.0	1.0	1.1	0.9	0.9	1.0	1.0	1.1	1.2	1.0	1.0	1.3	1.0	1.0	2.0	1.0	1.1	3.1	0.9	1.2	3.7
1367831_at	Tp53	1.0	0.9	0.9	1.0	1.0	1.0	1.0	1.1	1.3	1.1	1.3	1.2	1.3	1.0	1.3	1.3	1.3	2.0	1.3	1.0	2.4	0.8	1.2	2.0
1367890_at	Casp2	1.1	1.1	1.1	0.9	1.1	1.1	1.0	0.9	1.1	1.0	1.0	1.2	1.1	1.0	1.0	1.1	1.2	1.3	0.9	1.0	1.2	1.1	1.1	1.9
1368247_at	Hspa1a/1b	0.9	1.2	1.4	1.4	1.4	2.8	1.1	1.1	1.5	1.5	1.7	1.8	1.2	1.1	1.8	1.5	1.5	1.4	0.8	1.2	1.2	0.7	0.6	0.4
1368273_at	Mapk8	1.1	1.2	1.2	1.0	1.3	1.8	1.0	1.1	1.4	1.1	1.0	1.0	0.9	0.9	0.9	0.9	0.9	1.1	1.0	0.9	1.1	0.9	1.0	1.0
1368277_at	Ppp3ca	1.1	0.9	1.0	0.9	0.9	1.2	1.2	1.2	1.2	1.1	1.1	1.2	1.0	1.1	1.1	1.0	1.3	1.3	1.1	1.0	1.3	1.2	1.1	1.6
1368305_at	Casp8	0.9	0.9	0.9	0.9	1.0	1.1	1.1	1.2	1.2	0.9	1.0	1.4	1.3	1.0	1.4	1.0	0.9	1.1	1.0	1.1	1.1	0.9	1.1	1.8
1368308_at	Myc	2.0	2.1	3.9	0.7	0.8	3.6	0.7	1.1	1.8	0.8	0.8	1.4	2.0	1.5	1.8	1.5	1.6	2.8	1.9	2.4	5.1	0.9	1.4	3.4
1368862_at	Akt1	1.0	0.8	0.8	1.0	0.8	0.9	0.9	1.1	0.8	0.9	1.0	1.1	0.9	0.8	0.9	1.0	0.9	1.3	1.0	1.0	1.6	0.8	1.0	1.4
1368871_at	Map3k1	1.3	1.0	1.0	0.8	0.7	0.7	0.8	1.2	1.2	0.8	0.7	0.7	0.9	0.9	0.8	0.9	1.0	2.0	1.0	1.2	2.4	1.1	1.0	3.0
1368947_at	Gadd45a	1.3	1.3	5.3	0.6	0.7	2.5	0.8	0.9	1.2	0.8	0.9	1.8	1.1	0.8	1.4	1.1	1.3	3.4	0.6	1.3	3.7	1.5	2.1	7.6
1369590_a_at	Ddit3	1.0	1.3	4.3	1.1	1.1	3.0	1.1	0.9	1.3	1.0	1.1	1.2	0.9	1.0	1.2	0.7	1.0	3.0	0.9	1.2	5.3	1.1	1.3	7.1
1369653_at	Tgfbr2	1.0	1.0	0.9	0.6	0.9	0.7	0.8	1.7	1.5	1.1	1.1	1.0	1.3	1.1	1.4	1.1	1.2	6.5	0.8	2.0	3.2	0.8	1.7	3.2
1369932_a_at	Raf1	1.0	1.1	1.1	1.0	1.2	1.6	1.2	1.2	1.6	0.9	0.9	1.0	1.0	1.1	1.0	0.9	0.9	1.1	1.0	0.9	1.2	0.9	0.9	1.2
1370035_at	Kras2	0.9	0.9	0.8	1.1	1.2	1.5	1.1	1.2	1.5	1.0	0.9	1.1	1.0	1.1	1.0	1.0	1.0	1.3	0.9	1.0	1.2	0.9	1.0	1.3
1370265_at	Arrb2	0.8	0.9	1.2	1.2	1.1	1.1	0.6	1.0	0.8	0.8	0.8	1.2	1.2	1.1	1.1	1.0	1.4	2.4	1.0	0.8	1.6	0.8	1.2	3.2
1370427_at	Pdgfa	0.9	0.8	0.9	1.5	2.4	4.2	1.0	0.9	2.0	0.8	0.7	1.2	1.2	1.1	1.1	2.6	2.5	5.4	0.8	2.0	4.5	0.9	1.0	4.1
1370585_a_at	Prkcb1	0.9	1.0	1.1	1.0	0.9	1.2	1.3	1.0	1.0	0.8	0.9	1.3	1.5	0.9	0.9	0.9	1.0	1.4	1.0	1.0	1.4	1.1	1.2	2.2
1370825_a_at	Cdc42	1.0	0.9	1.0	1.0	1.1	1.0	1.1	1.1	1.1	1.0	1.0	1.1	1.0	1.1	1.1	1.0	1.0	1.3	1.0	1.1	1.5	1.0	1.1	1.5
1370968_at	Nfkb1	1.0	0.9	1.0	1.0	1.0	1.2	1.0	1.0	1.2	1.0	0.8	1.1	1.1	0.9	1.0	1.0	1.0	1.3	1.2	1.1	1.9	1.0	1.2	2.0
1372982_at	Ppp3r1	0.9	1.3	1.3	1.1	1.3	1.5	1.4	1.2	1.2	0.9	1.0	1.2	1.0	1.1	1.0	0.9	0.9	1.5	0.9	0.7	1.1	1.1	1.2	2.2
1375043_at	Fos	0.4	0.3	3.6	0.5	1.0	3.4	2.8	1.7	3.0	0.2	0.2	0.2	0.8	0.8	0.6	1.5	5.5	14	0.5	1.0	6.8	1.8	1.7	15
1376425_at	Tgfb2	1.2	1.1	1.0	1.1	1.4	1.0	1.2	1.0	1.0	1.2	1.3	1.2	1.1	1.0	1.0	1.0	0.9	1.6	1.1	1.1	2.1	1.1	1.3	2.8
1386935_at	Nr4a1	1.1	1.0	1.4	1.1	1.0	1.5	0.7	0.8	0.8	1.1	1.0	1.0	1.2	1.0	1.0	0.9	0.9	1.4	1.0	1.0	1.5	1.1	1.5	2.7
1387377_a_at	Pak1	0.7	0.8	0.9	1.6	1.3	1.5	0.5	0.3	0.6	0.5	0.8	0.9	1.4	0.8	1.2	1.5	0.8	1.4	0.9	2.2	5.1	0.4	0.7	2.8
1387498_a_at	Fgfr1	1.0	0.8	1.0	0.7	0.9	0.7	0.9	1.0	0.9	1.0	1.0	0.9	1.0	1.1	0.9	1.5	1.4	1.9	1.0	1.0	1.3	0.8	1.0	2.3
1387643_at	Fgf21	1.2	2.1	8.8	0.6	1.2	3.6	0.7	1.0	1.6	1.0	1.1	5.1	1.1	1.5	3.9	1.1	5.0	7.5	0.9	4.8	6.4	3.1	3.5	6.6
1387771_a_at	Mapk3	1.2	1.2	1.1	1.1	1.0	0.9	0.9	1.1	0.9	1.1	0.9	1.0	1.2	1.2	1.0	0.9	1.1	1.2	0.9	0.9	1.3	0.9	0.9	2.1
1387806_at	Rap1b	1.0	1.0	1.0	1.0	1.0	1.2	1.0	1.0	1.1	0.9	0.9	1.1	1.1	1.0	1.0	1.0	1.1	1.3	1.0	1.0	1.4	1.0	1.1	1.6
1389170_at	Casp7	1.0	0.9	0.9	0.9	1.0	0.8	0.9	1.0	1.0	1.0	1.0	1.2	1.0	1.0	1.1	1.0	1.1	1.3	1.0	1.0	1.5	1.1	1.2	1.6
1389528_s_at	Jun	1.3	1.3	3.4	0.9	0.6	2.0	0.8	0.8	1.5	0.9	0.5	0.9	1.5	1.5	1.3	1.7	1.4	2.3	0.7	1.4	1.6	1.4	1.4	2.8
1398240_at	Hspa8	0.9	1.3	1.2	1.0	1.1	1.6	1.2	1.2	1.5	1.2	1.2	1.2	1.0	1.0	1.2	1.0	1.1	1.1	0.9	0.9	1.2	0.9	0.9	1.1
1398256_at	Il1b	0.7	0.6	0.6	0.8	0.6	0.8	0.9	0.9	1.1	0.6	0.7	1.1	2.3	0.8	1.5	1.2	1.1	1.5	1.0	1.1	1.8	1.2	1.0	2.1

The number in each column expresses the ratio to control (N=3).

Fig. 5. Heatmap of individual gene expression change in category of "MAPK signaling".

AFFYMETRIX PROBE ID	SYMBOL	03H			06H			09H			24H			04D			08D			15D			29D		
		L	M	H	L	M	H	L	M	H	L	M	H	L	M	H	L	M	H	L	M	H	L	M	H
1367590_at	Ran	1.1	0.9	0.9	1.0	1.1	1.5	1.0	1.1	1.8	1.0	1.3	1.7	0.9	1.0	1.3	1.1	1.2	2.4	1.0	1.2	1.9	1.0	1.4	1.9
1367764_at	Ccng1	0.9	1.0	1.0	1.0	1.2	2.4	1.0	0.9	1.9	1.3	1.3	2.2	0.8	0.9	1.3	1.0	1.1	2.4	1.0	1.0	3.4	1.3	2.2	6.2
1367827_at	Ppp2cb	1.0	1.1	0.9	1.0	1.1	1.5	1.1	1.2	1.8	1.0	1.0	1.1	0.9	1.0	1.1	1.0	1.1	1.8	0.9	1.2	2.1	1.0	1.2	2.2
1367831_at	Tp53	1.0	0.9	0.9	1.0	1.0	1.0	1.0	1.1	1.3	1.1	1.3	1.2	1.3	1.0	1.3	1.3	1.3	2.0	1.3	1.0	2.4	0.8	1.2	2.0
1368076_at	Vhl	1.0	1.1	1.1	1.0	1.0	1.1	1.0	0.9	1.1	1.0	0.9	1.0	1.1	1.0	1.0	1.0	1.1	1.4	1.0	1.0	1.6	1.0	1.0	1.9
1368308_at	Myc	2.0	2.1	3.9	0.7	0.8	3.6	0.7	1.1	1.8	0.8	0.8	1.4	2.0	1.5	1.8	1.5	1.6	2.8	1.9	2.4	5.1	0.9	1.4	3.4
1368947_at	Gadd45a	1.3	1.3	5.3	0.6	0.7	2.5	0.8	0.9	1.2	0.8	0.9	1.8	1.1	0.8	1.4	1.1	1.3	3.4	0.6	1.3	3.7	1.5	2.1	7.6
1369590_a_at	Ddit3	1.0	1.3	4.3	1.1	1.1	3.0	1.1	0.9	1.3	1.0	1.1	1.2	0.9	1.0	1.2	0.7	1.0	3.0	0.9	1.2	5.3	1.1	1.3	7.1
1369932_a_at	Raf1	1.0	1.1	1.1	1.0	1.2	1.6	1.2	1.2	1.6	0.9	0.9	1.0	1.0	1.1	1.0	0.9	0.9	1.1	1.0	0.9	1.2	0.9	0.9	1.2
1369950_at	Cdk4	1.0	1.0	0.9	1.1	1.1	1.1	1.1	1.2	1.3	1.0	1.0	1.2	1.0	1.0	1.1	0.9	1.2	2.0	1.0	1.1	1.9	1.0	1.3	2.2
1369958_at	Rhob	0.9	1.0	1.7	1.0	1.0	3.9	1.2	1.1	1.9	0.8	0.7	0.9	0.9	1.0	1.1	1.0	1.1	2.0	1.2	1.3	3.0	1.0	1.5	3.9
1370035_at	Kras2	0.9	0.9	0.8	1.1	1.2	1.5	1.1	1.2	1.5	1.0	0.9	1.1	1.0	1.1	1.0	1.0	1.0	1.3	0.9	1.0	1.2	0.9	1.0	1.3
1370361_at	Cgref1	1.1	0.6	1.1	0.7	1.0	1.1	0.7	0.9	1.4	0.5	0.6	1.4	1.6	1.9	1.6	1.3	2.0	5.4	0.7	1.2	3.3	1.5	2.3	6.5
1370427_at	Pdgfa	0.9	0.8	0.9	1.5	2.4	4.2	1.0	0.9	2.0	0.8	0.7	1.2	1.2	1.1	1.1	2.6	2.5	5.4	0.8	2.0	4.5	0.9	1.0	4.1
1370504_s_at	Pmp22	1.2	1.5	1.2	0.8	0.9	1.1	0.7	0.7	0.6	0.8	0.8	1.0	1.2	1.4	1.3	1.3	1.6	1.6	1.1	1.3	1.5	1.8	1.4	2.7
1370809_at	Tubg1	1.1	1.0	0.9	1.0	1.0	1.1	1.0	0.9	1.0	1.0	1.0	1.4	1.1	1.2	1.1	1.1	1.0	1.5	0.9	1.2	2.2	1.2	1.5	2.6
1371308_at	Rps4x	1.0	1.0	1.0	0.9	1.0	1.0	1.0	1.0	1.1	1.0	1.1	1.2	1.0	1.0	1.1	1.0	1.1	1.6	1.1	1.3	1.6	1.2	1.3	1.6
1374966_at	Pcm1	1.2	0.9	1.1	0.9	0.9	0.9	1.3	1.1	1.2	1.0	1.1	1.0	1.0	0.9	0.9	1.2	1.2	1.4	1.0	0.9	1.3	1.1	0.9	1.6
1375630_at	RGD:1303103	1.0	0.8	1.0	1.0	1.1	1.3	1.1	1.0	1.4	1.0	1.1	1.3	0.9	1.0	1.0	1.2	1.2	1.6	1.1	1.2	1.9	1.0	1.2	1.8
1376425_at	Tgfb2	1.2	1.1	1.0	1.1	1.4	1.0	1.2	1.0	1.0	1.2	1.3	1.2	1.1	1.0	1.0	1.0	0.9	1.6	1.1	1.1	2.1	1.1	1.3	2.8
1379375_at	Pdgfa	1.1	1.1	1.1	1.0	1.2	2.0	0.9	0.9	1.6	0.7	0.8	1.1	1.2	1.1	1.3	0.3	1.0	1.9	0.9	0.9	2.1	1.1	1.3	3.0
1386866_at	Ywhag	1.1	1.0	1.1	0.9	1.2	1.9	1.1	1.3	1.9	1.1	0.9	1.1	1.0	1.0	1.2	1.1	1.2	1.7	1.0	1.1	1.8	1.0	1.2	2.2
1387391_at	Cdkn1a	0.9	1.1	0.9	1.1	1.5	3.9	0.6	0.7	2.8	1.2	2.2	2.9	1.2	1.1	1.4	1.9	2.5	5.9	1.1	2.1	3.1	0.9	2.8	2.5
1387616_at	Pdgfc	1.0	1.0	0.9	1.0	0.9	1.2	1.1	1.0	0.8	1.0	0.9	0.8	1.2	0.8	1.1	1.3	1.3	1.6	0.9	0.9	1.2	0.8	0.9	2.2
1387644_at	Btc	1.0	1.1	1.0	1.1	0.9	0.9	1.0	0.9	0.7	0.9	1.1	1.1	1.3	1.0	1.4	1.3	0.8	1.0	0.9	1.0	1.6	1.0	0.8	1.9
1387788_at	Junb	1.2	1.0	1.6	1.1	0.7	1.3	0.7	0.9	1.5	1.6	1.4	1.4	1.4	0.9	1.4	1.1	1.0	1.3	1.0	1.1	2.1	1.1	1.0	4.0
1388154_at	E2f5	1.0	1.0	1.1	1.0	1.4	1.7	1.0	1.1	1.7	1.2	1.1	1.2	1.0	1.0	1.1	1.1	1.1	1.4	1.0	1.0	1.5	0.9	1.1	1.7
1388808_at	Ppp2ca	1.1	1.0	1.0	1.1	1.0	1.4	1.1	1.0	1.4	0.9	1.0	1.5	1.2	1.1	1.5	0.9	1.0	1.7	0.8	1.0	2.7	1.1	1.3	3.6
1388867_at	MGC112830	1.0	1.1	1.2	0.9	1.1	1.4	1.0	1.1	1.1	0.9	0.9	1.0	1.0	1.1	1.1	0.9	1.1	1.3	1.0	1.0	1.2	0.9	1.0	1.7
1389101_at	Ccnc	0.7	0.7	0.5	0.9	1.1	1.2	1.2	1.0	0.8	1.2	1.1	1.4	1.2	1.1	1.1	1.1	1.3	2.0	1.3	1.6	2.5	1.5	1.6	2.5
1389528_s_at	Jun	1.3	1.3	3.4	0.9	0.6	2.0	0.8	0.8	1.5	0.9	0.5	0.9	1.5	1.5	1.3	1.7	1.4	2.3	0.7	1.4	1.6	1.4	1.4	2.8
1398240_at	Hspa8	0.9	1.3	1.2	1.0	1.1	1.6	1.2	1.2	1.5	1.2	1.2	1.2	1.0	1.0	1.2	1.0	1.1	1.1	0.9	0.9	1.2	0.9	0.9	1.1
1398256_at	Il1b	0.7	0.6	0.6	0.8	0.6	0.8	0.9	0.9	1.1	0.6	0.7	1.1	2.3	0.8	1.5	1.2	1.1	1.5	1.0	1.1	1.8	1.2	1.0	2.1

The number in each column expresses the ratio to control (N=3).

Fig. 6. Heatmap of individual gene expression change in category of "regulation of cell cycle".

of MP by focusing on the toxicological pathway drawn from transcriptome analysis. Genes up-regulated from the early stage described above would be promising candidates of biomarkers for hepatotoxicity. However, the present analysis focused on one chemical, MP. It is necessary to analyze other chemicals causing glutathione depletion/oxidative stress and nongenotoxic hepatocarcinogenesis, such as thioacetamide, coumarin and ethionine, in order to establish a useful and precise prediction system based on the toxicogenomics approach.

The greatest advantage of toxicogenomics in toxicology is that various toxicity mechanisms can be elucidated at once compared with the conventional strategy where many experiments are performed one by one. This strategy is so powerful that comprehensive seizure of what happens for the mechanism in the target organ is possible. Toxicogenomics enables one to supply supporting data for any conventional toxicological changes and suggests the appropriate toxicological mechanism behind them.

ACKNOWLEDGMENT

This work was supported in part by a grant from the Ministry of Health, Labour and Welfare (H14-Toxico-001).

REFERENCES

Althaus, F.R., Lawrence, S.D., Sattler, G.L. and Pitot, H.C. (1982): DNA damage induced by the antihistaminic drug methapyrilene hydrochloride. Mutat. Res., **103**, 213-218.

Chu, T.M., Deng, S., Wolfinger, R., Paules, R.S. and Hamadeh, H.K. (2004): Cross-site comparison of gene expression data reveals high similarity. Environ. Health Perspect., **112**, 449-455.

Corcoran, C.A., Luo, X., He, Q., Jiang, C., Huang, Y. and Sheikh, M.S. (2005): Genotoxic and endoplasmic reticulum stresses differentially regulate TRB3 expression. Cancer Biol. Ther., **4**, 1063-1067.

Fischer, G., Altmannsberger, M., Schauer, A. and Katz, N. (1983); Early stages of chemically induced liver carcinogenesis by oral administration of the antihistaminic methapyrilene hydrochloride. J. Cancer Res. Clin. Oncol., **106**, 53-57.

Hamadeh, H. K., Knight, B.L., Haugen, A.C., Sieber, S., Amin, R.P.,

Bushel, P.R., Stoll, R., Blanchard, K., Jayadev, S., Tennant, R.W., Cunningham, M.L., Afshari, C.A. and Paules, R.S. (2002): Methapyrilene toxicity: Anchorage of pathologic observations to gene expression alterations. Toxicol. Pathol., **30**, 470-482.

Kiyosawa, N., Shiwaku, K., Hirode, M., Omura, K., Uehara, T., Shimizu, T., Mizukawa, Y., Miyagishima, T., Ono, A., Nagao, T. and Urushidani, T. (2006): Utilization of a one-dimensional score for surveying the chemical-induced changes in expression levels of multiple biomarker gene sets using a large-scale toxicogenomics database. J. Toxicol. Sci., **31**, 433-448.

Kiyosawa, N., Uehara, T., Gao, W., Omura, K., Hirode, M., Shimizu, T., Mizukawa, Y., Ono, A., Miyagishima, T., Nagao, T. and Urushidani, T. (2007): Identification of glutathione depletion-responsive genes using phorone-treated rat liver. J.Toxicol. Sci., **32**, 469-486.

Lijinsky, W., Reuber, M.D. and Blackwell, B.N. (1980): Liver tumors induced in rats by oral administration of the antihistaminic methapyrilene hydrochloride. Science, **209**, 817-819.

Mirsalis, J.C. (1987): Genotoxicity, toxicity, and carcinogenicity of the antihistamine methapyrilene. Mutat. Res., **185**, 309-317.

NTP Hepatotoxicity Studies of the Liver Carcinogen Methapyrilene Hydrochloride (CAS No. 135-23-9) Administered in Feed to Male F344/N Rats. Toxic Rep Ser. 46:1-C7, 2000.

Ratra, G.S., Morgan, W.A., Mullervy, J., Powell, C.J. and Wright, M.C. (1998): Methapyrilene hepatotoxicity is associated with oxidative stress, mitochondrial disfunction and is prevented by the Ca^{2+} channel blocker verapamil. Toxicology, **130**, 79-93.

Ratra, G.S., Powell, C.J., Park, B.K., Maggs, J.L. and Cottrell, S. (2000): Methapyrilene hepatotoxicity is associated with increased hepatic glutathione, the formation of glucuronide conjugates, and enterohepatic recirculation. Chem. Biol. Interact., **129**, 279-295.

Snedecor, G.W. and Cochran, W.G. (1989): Statistical Methods, 8th ed., Iowa State University Press.

Steinmetz, K.L., Tyson, C.K, Meierhenry, E.F., Spalding, J.W, and Mirsalis, J.C. (1988): Examination of genotoxicity, toxicity and morphologic alterations in hepatocytes following *in vivo* or *in vitro* exposure to methapyrilene. Carcinogenesis, **9**, 959-963.

Turner, N.T., Woolley, J.L. Jr., Hozier, J.C., Sawyer, J.R. and Clive, D. (1987): Methapyrilene is a genotoxic carcinogen: Studies on methapyrilene and pyrilamine in the L5178Y/TK +/– mouse lymphoma assay. Mutat. Res., **189**, 285-297.

Urushidani, T. and Nagao, T. (2005): Toxicogenomics: The Japanese initiative. In Handbook of Toxicogenomics - Strategies and Applications. (Borlak, J., ed.), pp. 623-631. Wiley-VCH.

Waring, J.F., Ulrich, R.G., Flint, N., Morfitt, D., Kalkuhl, A., Staedtler, F., Lawton, M., Beekman, J.M. and Suter, L. (2004): Interlaboratory evaluation of rat hepatic gene expression changes induced by methapyrilene. Environ. Health Perspect., **112**, 439-448.

In Vitro Cell.Dev.Biol—Animal
DOI 10.1007/s11626-007-9021-9

Chromosomal instability in human mesenchymal stem cells immortalized with human papilloma virus E6, E7, and hTERT genes

Masao Takeuchi · Kikuko Takeuchi · Arihiro Kohara · Motonobu Satoh · Setsuko Shioda · Yutaka Ozawa · Azusa Ohtani · Keiko Morita · Takashi Hirano · Masanori Terai · Akihiro Umezawa · Hiroshi Mizusawa

Received: 25 January 2007 / Accepted: 27 March 2007 / Editor: J. Denry Sato

Abstract Human mesenchymal stem cells (hMSCs) are expected to be an enormous potential source for future cell therapy, because of their self-renewing divisions and also because of their multiple-lineage differentiation. The finite lifespan of these cells, however, is a hurdle for clinical application. Recently, several hMSC lines have been established by immortalized human telomerase reverse transcriptase gene (hTERT) alone or with hTERT in combination with human papillomavirus type 16 E6/E7 genes (E6/E7) and human proto-oncogene, Bmi-1, but have not so much been characterized their karyotypic stability in detail during extended lifespan under in vitro conditions. In this report, the cells immortalized with the hTERT gene alone exhibited little change in karyotype, whereas the cells immortalized with E6/E7 plus hTERT genes or Bmi-1, E6 plus hTERT genes were unstable regarding chromosome numbers, which altered markedly during prolonged culture. Interestingly, one unique chromosomal alteration was the preferential loss of chromosome 13 in three cell lines, observed by fluorescence in situ hybridization (FISH) and comparative-genomic hybridization (CGH) analysis. The four cell lines all maintained the ability to differentiate into both osteogenic and adipogenic lineages, and two cell lines underwent neuroblastic differentiation. Thus, our results were able to provide a step forward toward fulfilling the need for a sufficient number of cells for new therapeutic

M. Takeuchi (✉) · K. Takeuchi · A. Kohara · S. Shioda · Y. Ozawa · A. Ohtani · H. Mizusawa
Division of Bioresources,
National Institute of Biomedical Innovation,
Osaka 567-0085, Japan
e-mail: takeuchim@nibio.go.jp

K. Takeuchi
e-mail: takeuchik@nibio.go.jp

A. Kohara
e-mail: kohara@nibio.go.jp

S. Shioda
e-mail: shioda@nibio.go.jp

Y. Ozawa
e-mail: ozaway@nibio.go.jp

A. Ohtani
e-mail: aohtani@nibio.go.jp

H. Mizusawa
e-mail: mizusawa@nibio.go.jp

M. Satoh
Health Science Research Resources Bank,
Osaka 590-0535, Japan
e-mail: satoh@osa.jhsf.or.jp

K. Morita · T. Hirano · A. Umezawa
National Research Institute for Child Health and Development,
Tokyo 157-8535, Japan

K. Morita
e-mail: morita-keiko@aist.go.jp

T. Hirano
e-mail: hirano-takashi@aist.go.jp

A. Umezawa
e-mail: umezawa@1985.jukuin.keio.ac.jp

M. Terai
Department of Reproductive Biology
and Pathology and Innovative Surgery,
National Research Institute for Child Health and Development,
Tokyo 157-8535, Japan
e-mail: terai@nch.go.jp

applications, and substantiate that these cell lines are a useful model for understanding the mechanisms of chromosomal instability and differentiation of hMSCs.

Keywords Human cord blood mesenchymal stem cell · Long-term culture · Karyotype analysis · mFISH CGH · Differentiation

Introduction

Tissue-specific stem cells in various adult tissues are known to be an important source in the regeneration of damaged tissue and maintenance of homeostasis in the tissues in which they reside. Among these stem cells, human mesenchymal stem cell (hMSC) has recently become of great interest in regenerative medicine, not only to replenish their own tissues, but also to give rise to more committed progenitor cells, which can differentiate into other tissues. MSCs in bone marrow have been shown to differentiate into several types of cell such as osteoblasts, adipocytes, chondrocytes, myocytes, and probably also neuronal cells (Okamoto et al. 2002; Takeda et al. 2004; Mori et al. 2005; Saito et al. 2005; Terai et al. 2005). Because of these properties, it is expected that hMSCs are an enormous potential source for future cell therapy. The goal of our study is to establish cell lines with long lifespan and with parental properties for clinical application. However, clinical application using these cells has been met with enormous difficulty, e.g., isolation of a cell population with specific criteria, expansion in vitro system for obtaining a sufficient number of cells without affecting their genomic characteristics and differentiation properties, and their storage in higher viability.

At present, there is a little evidence suggesting whether changes in these properties occur during expansion. Human normal MSCs have a limited capacity to replicate in the 40- to 50-population doubling level (PDL) at the most. To extend their lifespan, we have previously established human mesenchymal cell lines from human umbilical cord blood or bone marrow by immortalization with human telomerase reverse transcriptase (hTERT), human papillomavirus high-risk type 16 E6/E7 genes (HPV16E6/E7) or polycomb gene, Bmi-1 (Takeda et al. 2004; Mori et al. 2005; Terai et al. 2005).

hTERT-immortalization without affecting biological characteristics, despite extensive proliferation, has been reported in bone-marrow-derived hMSCs (Burns et al. 2005), human fibroblast (Milyavsky et al. 2003), and human keratinocyte (Harada et al. 2003), although it has been indicated that there is the possibility that prolonged culture of hTERT-immortalized fibroblasts may favor the appearance of clones carrying potentially malignant alterations (Milyavsky et al. 2003). HPV16, which encodes oncogenes (E6 and E7), can also immortalize hMSC's in vitro. Both E6 and E7 proteins act through their association with tumor suppressor gene products, p53 and retinoblastoma family members (pRb), respectively. E6 accelerates the degradation of the p53 protein, which is essential for cell arrest at the checkpoint in G_1/S and at the mitotic checkpoint when tetraploidy occurs (Cross et al. 1995), as well as at the G_2 phase under damaging conditions. E7 protein binds to pRb and abrogates the repressive function of these cell cycle regulations (Zheng et al. 2001). Thus, both p53 and pRb play a multitude of important roles in cell-cycle-progression checkpoints as reported in human keratinocytes (Patel et al. 2004), and fibroblasts (Khan et al. 1998). As a consequence, the disruption of the checkpoints that govern accurate cell division leads to abnormal segregation of chromosome and genomic instability, as shown in the cells immortalized with HPV16E6/E7 genes (Duensing et al. 2002).

In this paper, we report on the chromosomal instability and the differentiation activity during prolonged culture (cell expansion) using four mesenchymal stem cell lines. These results indicate that an umbilical cord blood-derived clone immortalized with hTERT (UCBTERT-21) showed normal karyotype for a period of 1 yr, whereas three other cell lines immortalized with HPV16E6/E7 and hTERT or HPV16E6, Bmi-1 and hTERT showed chromosomal instability but maintained the ability to differentiate.

Materials and Methods

Cell culture. Human mesenchymal stem cell lines, UCB TERT-21 (JCRB1107), UCB408E6E7TERT-33 (JCRB1110), UE6E7T-3 (JCRB1136), and UBE6T-6 (JCRB1140) were obtained from the JCRB Cell Bank (Osaka, Japan). Two of them are cell lines obtained by immortalizing human umbilical cord blood mesenchymal stem cells (UCB) with hTERT alone (UCBTERT-21; Terai et al. 2005) or with HPV16E6/E7 in combination with hTERT (UCB408E6E7TERT-33; Terai et al. 2005), and the two others are human bone-marrow-derived mesenchymal stem cell lines transformed with HPV16E6/E7 and hTERT genes (UE6E7T-3; Mori et al. 2005) or with bmi-1, HPV16E6 and hTERT genes (UBE6T-6; Takeda et al. 2004; Mori et al. 2005).

The UCBTERT-21 and UCB408E6E7TERT-33 were grown in PLUSOID-M medium (Med-Shirotori Co., Tokyo, Japan) or MSCGM BulletKit (Cambrex Co., East Rutherford, NJ). UE6E7T-3 and UBE6T-6 were cultured in POWEREDBY10 medium (Med-Shirotori Co.) or MSCGM BulletKit (Cambrex Co.); 5×10^3 cells/ml of each cell line were seeded and cultured for 7–10 d. When culture

plate was subconfluent, cells were treated with 0.25% trypsin/0.5 mM EDTA solution (both from Invitrogen, Tokyo, Japan) and replated at a density of 5×10^3 cells/mL.

All of the cells were maintained in a humidified incubator at 37° C and 5% CO_2. PDLs were calculated using the formula: PDL= log (cell output/input)/log2. At the starting cultivation, PDLs of UCBTERT-21, UCB408E6E7 TERT-33, UE6E7T-3, and UBE6T-6 were 42, 67, 60, and 56, respectively. The doubling time of the UCB408E6E7T-33 cell was 1.5 d, and that of UCBTERT-21, UE6E7T-3, or UBE6T-6 was 2.6, 2.0, or 4.0 days, respectively.

Measurement of chromosome number and fluorescence in situ hybridization. Metaphase chromosome spreads for measurement of chromosome number and fluorescence in situ hybridization (FISH) were prepared from exponential growing cells at various PDL. The cells were treated in a hypotonic solution after exposure to 0.06 μg/ml colcemid (Invitrogen, Carlsbad, CA) for 2 h and fixed in methanol/acetic acid (3:1). The cells were spread on a microscope slide.

To count the number of chromosomes, the cells were stained with DAPI (4′-6-diaminido-2-phenylindol; Vector Laboratories, Inc. Burlingame, CA) and examined under an Axioplan II imaging microscope (Carl Zeiss, GmbH) equipped with Leica QFISH software (Leica Microsystems Holding, UK). To examine statistically significant chromosome numbers, we have allowed ±1 deviation and 50–100 metaphase spreads were scored for each assay.

Painting probes specific for chromosome 13 (XCP13-kit; FITC; MetaSystems, GmbH) and chromosome 17 (XCP17-kit; Texas Red) (MetaSystems GmbH, Altlussheim, Germany), and multicolor probes (mFISH-24Xcyte-kit, DAPI, FITC, TexasRed, Cy3, Cy5, and DEAC; MetaSystems GmbH) were used for FISH analysis. FISH was performed according to the manufacture's protocol (MetaSystems GmbH). Briefly, both the metaphase chromosome spread and the probe were denatured with 0.07 N NaOH or 70% formamide, hybridized at 37° C for 1–4 d, and counterstained with DAPI. FISH images were captured and analyzed on the Zeiss Axio Imaging microscope (Carl Zeiss Microimaging GmbH, Jena, Germany) with Isis mBAND/mFISH imaging Software (MetaSystems GmbH).

CGH analysis. Hybridization was carried out with the BAC Array (MAC ArrayTM Karyo 4000 Component, Macrogen Co., Rockville, MD) by the Hybstation (Genomic Solutions, Ann Arbor, MI). Briefly, test DNAs, which were isolated using an isolation kit (Amersham BioSciences, Little Chalfont, UK) and Spin Column (QIAGEN Co., Tokyo, Japan), and reference DNAs (Promega Co., Madison, WI), were labeled, respectively, with Cy3 or Cy5 (BioPrimer DNA Labeling System, Invitrogen Co.), precipitated together with ethanol in the presence of Cot-1 DNA, redissolved in a hybridization mixture (50% formamide, 10% dextran sulfate, 2xSSC, 4% sodium dodecyl sulfate [SDS], pH 7), and denatured at 75° C for 10 min. After incubation at 37° C for 30 min, each mixture was applied to an array slide and incubated at 42° C for 48–72 h. After hybridization, the slides were washed in a solution of 50% formamide—2× SSC (pH 7.0) for 15 min at 50° C, in 2× SSC—0.1% SDS for 15 min at 50° C, and in a 100-mM sodium phosphate buffer containing 0.1% Nonidet P-40 (pH 8) for 15 min at room temperature, then scanned with GenePix4000A (Axon Instruments, Union City, CA). Acquired images were analyzed with MacViewer (Macrogen Instruments).

Differentiation ability. To evaluate the differentiation potential of each cell line, cells were cultured on a coverslip in each induction medium, that is, hMSC Differentiation BulletKit-Adipogenic (PT-3004, Cambrex BioScience, Inc., Walkersville, MD) for adipocyte and NPMM Bullet kit (NPMM™ BulletKit (B3209, Cambrex BioScience) for neural progenitor cells. For osteoblast, cells were treated with 0.1 μM dexamethasone (Sigma Chemical Co., St. Louis, MO), 50 μg/ml L-ascorbic acid (Sigma Chemical), and 10 mM β-glycerophosphate (Sigma Chemical) in the PLUSOID-M medium (Med-Shirotori Co.) or the POWER-EDBY10 medium (Med-Shirotori Co.) of culture medium.

After 2–4 wk, the cells were washed in phosphate-buffered saline (PBS), fixed in 4% paraformaldehyde in PBS and stained with Oil Red-O (Sigma Chemical) for detection of adipocyte, and with alkaline phosphatase staining solution containing 0.25 mg/ml naphthol AS-BI phosphate and 0.25 mg/ml Fast violet LB salt for detection of alkaline phosphatase-positive osteoblast. In immunostaining for neuron-like cells, the cells fixed with paraformaldehyde were permeabilized with methanol at −20° C for 10 min and stained with an anti-IIIβ tubulin antibody (Sigma Chemical) or anti-neurofilament antibody NF-200 (Sigma Chemical) and Texas Red-anti-mouse IgG (Southern Biotechnology Associates, Inc., Birmingham, AL) as previously described (Takeuchi et al. 1990).

Results

Changes in chromosomal number in human mesenchymal stem cell lines in prolonged culture. Immortalization of cultured cells frequently induces an abnormal chromosome number as shown in cancer cells (Duensing et al. 2000; Munger et al. 2004; Patel et al. 2004), especially at higher frequency in long-term culture. We therefore examined four cell lines, human mesenchymal stem cell (hMSC) lines immortalized with combinations of bmi-1, E6, E7, and/or hTERT genes, for chromosome instability by counting metaphase chromosomes.

All of the lines were diploid, each containing 46 up to 40 PDL including the PDL numbers of nontransfecting original MSCs (Takeda et al. 2004; Mori et al. 2005; Terai et al. 2005). For UCBTERT-21 cell, no further changes in chromosome number have been observed up to date (for PDL 133) as shown in Fig. 1*A* and *B*. In contrast, although the UBE6T-6 cell and the UE6E7T-3 cell were near diploid, both cells exhibited considerable variation in chromosome number from PDL 70 after the culture started. For example, when the assay of UE6E7T-3 cells start at PDL 62 in culture, 90% of cell population had 46 chromosomes, but the population decreased with prolonged culturing and a population containing 44 chromosomes became dominant (43% of cell populations) at PDL 147 (Fig. 1*E*, *F*). A similar variation was also observed in UBE6T-6 cells (Fig. 1*C*, *D*).

To ascertain whether or not the changes observed were induced by transfection with HPV16E6E7, we assayed the chromosome numbers of UCB408E6E7TERT-33 cell in prolonged culture. The cell line showed similar chromosomal changes to those of the UE6E7T-3 cell, the rate of which was more rapid. At day 2 after culture by us changes became evident (PDL 68), the UCB408E6E7TERT-33 cells consisted of two distinct populations concerning chromosome number (near diploid [24%] and near tetraploid [53%]), shown in Fig. 1*G*. However, the near diploid population was unstable and decreased gradually. At PDL 81, the population became only near tetraploid, 80% of the

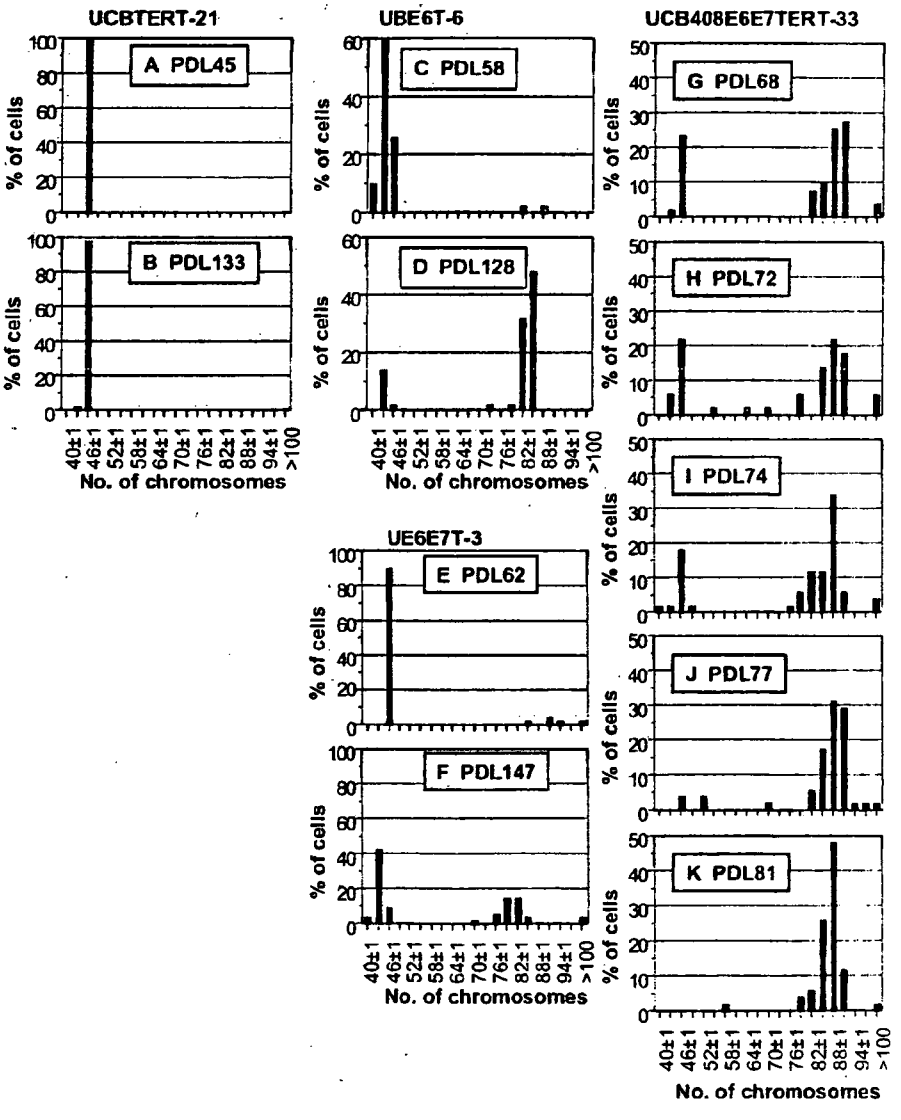

Figure 1. Changes in chromosomal numbers in prolonged cultures of four hMSC cell lines. (*A–K*) The chromosomal numbers at various culture stages were counted by DAPI staining. (*A*, *B*), (*C*, *D*), (*E*, *F*), and (*G–K*) represent the chromosomal numbers from UCBTERT-21, UBE6T-6, UE6E7T-3, and UCB408E6E7TERT-33, respectively. To examine statistically significant chromosomal numbers, we have allowed ±1 deviation, and 50–100 metaphase spreads were examined for each assay. *Note* the changes in chromosomal number from near 2*n* to near 4*n* in prolonged culture.

cells contain 85–92 chromosomes (Fig. 1*K*). The results indicate that UCBTERT-21 is relatively stable in chromosome number, whereas each of the oncogene-immortalized cells (UE6E7T-3, UBE6T-6, and UCB408E6E7TERT-33 cell) were unstable in chromosome numbers, which altered substantially during prolonged culture.

We next applied FISH and CGH analysis to characterize the chromosomal aberrations of the cell lines. All of the four cell lines passed for PDL 50 before examination by FISH. mFISH analysis of the UCBTERT-21 cell at PDL 52 showed normal chromosome composition (Fig. 2*A* and *B*) as observed in non-immortalized cells. The UBE6T-6 cell containing 43–45 chromosomes demonstrates losses of chromosome 13, 16, and 19 (marginal variation in chromosome 4 was observed among cells), but keeps on proliferating in chromosome number of 43–45 (Fig. 2*D*, *E*). In contrast, the UCB408E6E7TERT-33 cell showed more heterogeneity in chromosome composition with intrachromosomal and interchromosomal aberrations (data not shown). However, by mFISH analysis we were able to detect nonrandom losses of chromosome 13 in three cell lines except the UCBTERT-21 cell line. This was also confirmed by pFISH analysis using the probes specific for chromosome 13 and chromosome 17 (Fig. 2*C*, *F*). More than 97% of UCBTERT-21 cells showed two copies for chromosome 13, indicating the stability of the chromosomes in the cell line (Fig. 2*G*). The UE6E7T-3 and the UBE6T-6 cell lines with chromosome numbers of 43–45 showed only one copy of chromosome 13 in 76% of UE6E7T-3 cells and 86% of UBE6T-6 cells, respectively (Fig. 2*I*, *J*). A similar loss of chromosome 13 was also observed in 70% of UCB408E6E7TERT-33 cells, which showed three copies of chromosome 13 in near tetraploid (Fig. 2*H*). Other chromosomes, for example chromosome 17, were contained in the UCBTERT-21 and UBE6T-6 cell lines (Fig. 2*C*, *F*).

Furthermore, a significant nonrandom loss of chromosome 13 at the single cell-level observed by FISH was examined by array CGH, which samples the entire cell population. Figure 3 shows the array CGH profiles from early (*blue spots*) and late (*red spots*) stages of proliferating of each cell line. The UCBTERT-21 cell did not show any detectable differences in array CGH profiles between early and late stages (Fig. 3*A*). Although the loss of chromosome 13 had already occurred at early stages in the UBE6T-6 and the UCB408E6E7TERT-33 cell lines, in addition to the losses of chromosomes 4, 9, and 16 (Fig. 3*B*, *D*), in UE6E7T-3 the loss appeared between PDL 78 to 101 with loss of chromosome 16. The most compelling observation was that all three cell lines revealed a consistent whole loss of chromosome 13. These data are consistent with the results observed by FISH analysis. From these results, we

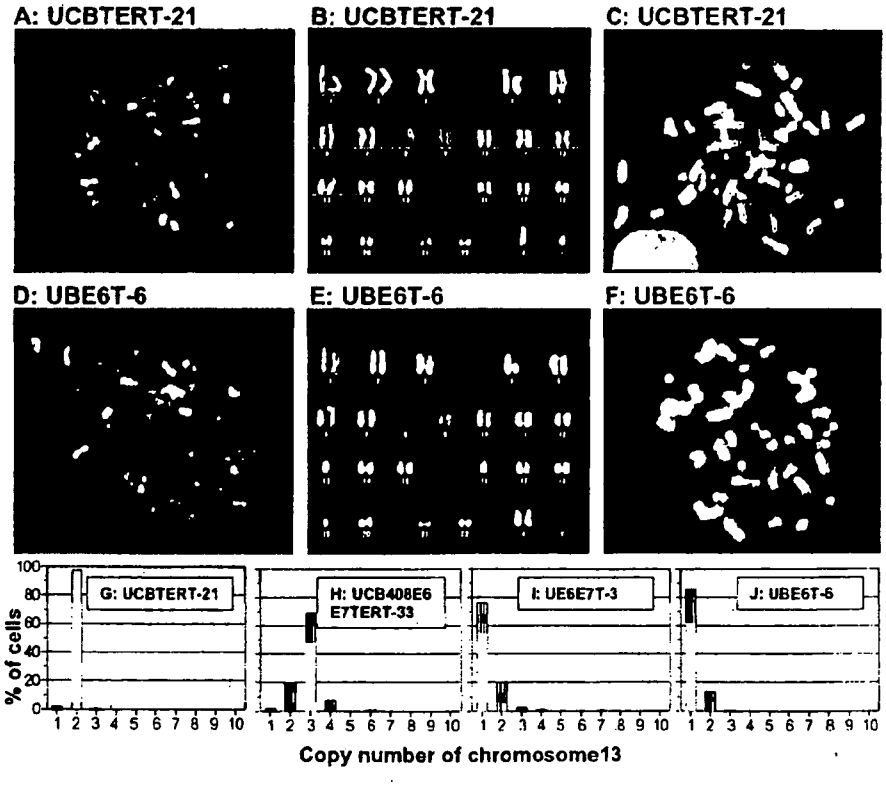

Figure 2. FISH analysis of human mesenchymal stem cell (hMSC) lines immortalized with hTERT alone, hTERT plus bm-1, HPVE6 or with hTERT plus HPVE6/E7. Multicolor FISH images of metaphase spreads (*A*, *D*), their karyotypes (*B*, *E*), and painting FISH images using DNA probes specific for chromosome 13 (*green*) and 17 (*red*) (*C*, *F*) of UCBTERT-21 (*A*, *B*, *C*) and UBE6T-6 (*D*, *E*, *F*). Quantity of chromosome 13 copy numbers in four cell lines (*G–J*). FISH signals were counted in 120–200 metaphase spreads plus interphase nuclei. UCBTERT-21 cells contained two copies of chromosome 13 and 17, and showed normal human karyotype, whereas other cells lost one copy of chromosome 13.

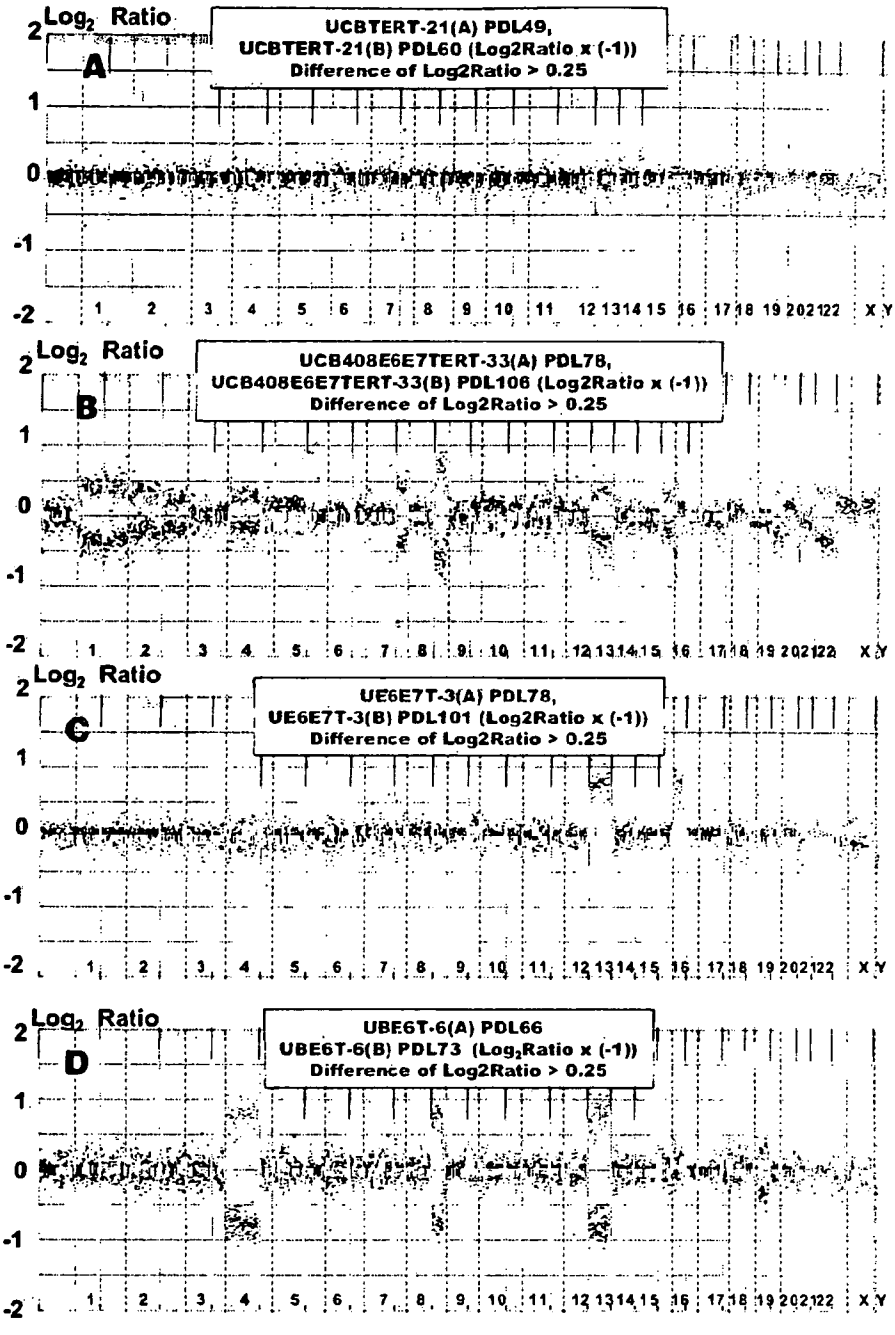

Figure 3. Array CGH profiles performed on four immortalized human mesenchymal stem cell lines at selected PDL. For each *panel*, the *X*-axis represents the 22 autosomes, the *X* and *Y* chromosomes, and the *Y*-axis shows the $\log_2$ of the fluorescence intensity ratio (cy3 [hMSCs]/cy5 [normal cell]) of all spots of the chromosome. Values above 0 (*red spots*) or values below 0 (*blue spots*) signify a loss of chromosome (chromosome regions). *Blue spots* in each *panel* indicate the $\log_2$ ratios observed at early stage in the culture of each cell line, which are overlaid with *red spots* indicated at the late stage. *Green spots* indicate the difference in value between *blue spots* and *red spot*. *Note* that in the UE6E7T-3 cell line, one copy of chromosome 13 and 16 were lost between PDL 78 and 101.

concluded that only hTERT-mediated immortalization induced little change in the chromosome numbers and chromosome structures of mesenchymal stem cells, but immortalization with Bmi-1, E6, and E7 in addition to hTERT results in chromosome instability.

Differentiation potential into lineages of immortalized mesenchymal stem cell lines. It has been reported that mesenchymal stem cells have the extensive potential to differentiate into multiple cell lineages including osteoblast, chondrocytes, adipocytes (Pittenger et al. 1999), cardiac myocytes (Makino et al. 1999), and neural cells (Pacary et al. 2006; Wislet-Gendebien et al. 2005). To evaluate whether chromosome instability of these cell lines in prolonged culture affects differentiation, cells of each cell line were stimulated in each induction medium for 2 to 4 wk. In

adipocyte-specific culture medium, all cell lines accumulated lipid-rich vacuoles in their cytoplasm within 2 wk, which were made evident by Oil Red-O staining. In particular, the UE6E7T-3 cell line showed a greater adipogenetic ability among the four cell lines (Fig. 4*Ab*). In osteoblast induction medium for 2 wk, UCB408E6E7 TERT-33 cells showed a marked increase in alkaline phosphatase expression, a marker of osteoblast, compared with those in the three other cell lines (Fig. 4*Ad*). In addition, UBE6T-6 cells in neuron induction medium reduced proliferation and displayed marked changes in morphology from being a flat-polygonal shape to taking on the characteristic neuron-like shape in which the cells develop long branching processes. Moreover, in comparing the expression patterns of characteristic neural antigens, i.e., neurofilament, III-β-tubulin, before and after induction (28 d), the pseudo-neural shaped cells showed apparent increases in immunoreactivity to both antibodies (Fig. 4*Af, Ah*),

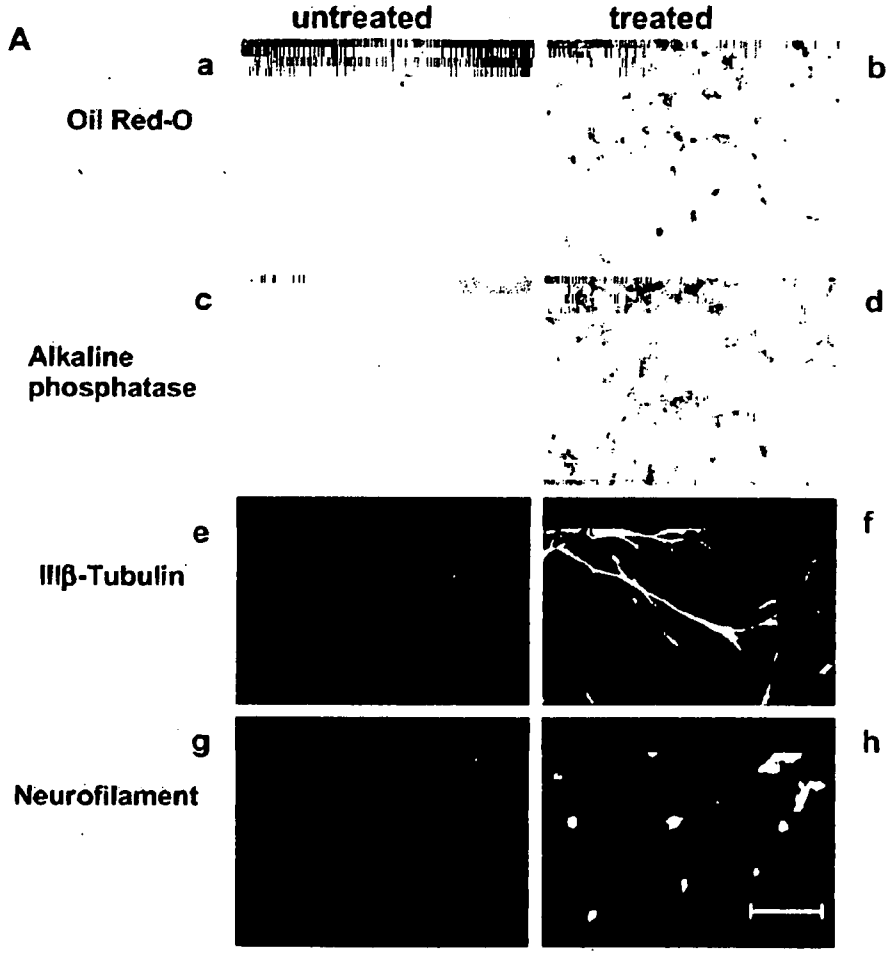

Figure 4. Differentiation potential of immortalized human mesenchymal stem cell lines into adipogenic, osteogenic, and neurogenic lineages. Adipogenesis was indicated by the accumulation of lipid stained with Oil Red-O (*Aa* and *Ab*, UE6E7T-3 cell line). Osteogenesis is indicated by the increase in alkaline phosphatase (*Ac* and *Ad*, UCB408E6E7TERT-33 cell line). Neurogenesis was shown by staining with two kinds of monoclonal antibodies to IIIβ-tubulin and neurofilament, and by shape changes of cell (*Ae–Ah*, UBE6T-6 cell line). *B*, Comparison of the differentiation potential of four cell lines whose responses to stimuli into differentiation were diverse among the cell lines. - and + indicate a response similar to an untreated cell and a weak positive response. +++ indicates a strong response shown by images of treated cells in Fig. 4*A*. (*Bar* indicates 20 μm).

B

	UCBTERT-21	UCB408E6E7TERT-33	UE6E7T-3	UBE6T-6
Oil Red-O	+	++	+++	+
Alkarine phosphatase	+	+++	+	+
IIIβ- Tubulin	-	+	+/-	+++
Neurofilament	-	++	-	++

whereas such changes were not evident with the flat-shaped cells before induction (Fig. 4*Ae*, *Ag*). Additionally, such cells did not undergo such differentiation in culture medium when cultured for as long as 30 d, although faint staining was observed. Figure 4*B* shows the overall results of differentiation potential of the four cell lines into adipogenic, ostcogenic, and neurogenic lineages. These immortalized mesenchymal stem cell lines retained the ability to differentiate into three lineages, although among cell lines there are significant variations in response to lineage-specific induction.

Discussion

Attempts to clarify the mechanisms for extending the lifespan of tumor cells have been made for many years, and several genes that have effects on cellular proliferation and survival have become clear (Munger et al. 2002) in addition to the elucidation that the majority of tumor cells express telomerase (hTERT; Armanios et al. 2005). The goal of one of the series of our studies has been to establish cell lines with long lifespan and with parental properties, on the basis of genotypic and phenotypic characterizations, for application to cell-based therapy. We previously established several cell lines (Takeda et al. 2004; Mori et al. 2005; Terai et al. 2005), and the present study demonstrated that UCBTERT-21, the immortalized cell line derived from human umbilical cord blood-derived MSCs with hTERT, has a normal karyotype and has an extended lifespan by at least 133 population doublings, and has the differentiation potential into the adipocyte or osteoblast similar to parental MSCs (Terai et al. 2005), although the potential was weak but clearly positive in this study. The specific environmental cues to initiate the differentiation of hMSCs are not yet clear.

UCBTERT-21 immortalized with hTERT alone can be prolonged without inhibition of the $p16^{INK4A}$/RB pathway (Terai et al. 2005), the result of which is in agreement with reports that hTERT alone significantly extends the lifespan of human fibroblasts, epithelial, and endothelial cells (Bodnar et al. 1998; Chang et al. 2005), without the requirement for molecular alterations in p53/p21 and pRB/$p16^{INK4A}$ pathways (Milyavsky et al. 2003). However, other researchers have indicated that inactivation of the RB/p16 pathway by E7, or downregulation of p16 expression, in addition to increasing telomerase activities, is necessary for expanding the lifespan of human keratinocytes (Dickson et al. 2000; Kiyono et al. 1998). Thus, the possibility that a telomere-independent barrier may operate to prevent immortalization according to cell types has been indicated.

UCB408E6E7TERT-33, UE6E7T-3, and UBE6T-6 are hMSC-clones immortalized with HPV16E6/E7 or polycomb group oncogene Bmi-1, in combination with hTERT Immortalization of human keratinocyte in vitro using virus-derived oncogenes such as E6 and E7 is based on initial inactivation of the p53 and/or Rb pathways, which are essential for controlling cell cycle progression in response to DNA damage or after induction tetraploidy; therefore, this gene transduction induces chromosomal abnormalities (Solinas-Toldo et al. 1997; Duensing et al. 2002; Patel et al. 2004; Schaeffer et al. 2004). The cell lines used in this study became completely immortal, yet underwent dynamic changes in their chromosome numbers in prolonged culture. Near diploid population in early passage of UCB408E6E7 TERT-33 became near-tetraploid population with prolonged culture without the appearance of intermediate populations (60–70 chromosomes/cell), and thereafter gave rise to a population having smaller numbers of chromosomes than tetraploid. Similar patterns existed, although at a slower rate, in UBE6T-6 cells and UE6E7T-3. These results suggest that HPVE6 and E7 proteins cause tetraploidy that precedes the chromosomal aberration to aneuploid in E6/E7-immotalized hMSCs, as is currently shown in several lines of evidence. For example, in vitro experiments in human cell lines (N/TERT-1 keratinocytes and HeLa cells) demonstrate that chromosome nondisjunction yields tetraploid rather than aneuploid, and that aneuploid may develop through chromosomal loss from tetraploid, although the mechanistic basis for the tetraploid formation still remains to be elucidated (Shi et al. 2005). This is also suggested from evidence that high frequency of tetraproidy is present with aneuploidy in human tumors (Olaharski et al. 2006; Sen 2000). A distinct pattern of aneuploid became apparent using dual-probe FISH and CGH analyses, in which UCB408E6E7TERT-33 cells predominantly exhibited triploid 13 and tetraploidy 17 together with other chromosomal changes as shown in Figs. 2 and 3. However, surprisingly, the loss of one copy of chromosome 13 was also seen in 70–80% of diploid UE6E7T-3 and diploid UBE6T-6 cells retaining two copies of chromosome 17. The loss occurred in PDL 50 in both UE6E7T-6 and UCB408E6E7TERT-33, and between PDL 78 and 101 in UE6E7T-3. Structural and numerical aberrations targeting chromosome 17 are often reported in tumors from various tissues (Olaharski et al. 2006), whereas the pattern that chromosome 13 is lost and chromosome 17 is stable, was common for the three cell lines in this study, indicating the possibility that the loss of chromosome 13 may play an important role in the chromosomal aberration of hMSC's to acquire growth advantages under the given culturing condition. Similar karyotypic changes were evident in cultured human embryonic stem cells, involving the gain of chromosome 17 or chromosome 12 (Carlson et al. 2000; Draper et al. 2004). It is thus conjectured that the aneuploidy developed through chromosomal loss from

diploid cells arises through different mechanisms from tetraploid intermediate.

An alternative explanation for aneuploid formation mechanism independent of tetraploid intermediate is loss of regulation in centrosome duplication, leading to abnormal centrosome amplification and multipolar spindles, resulting in aneuploidy. In addition, centrosome amplification caused by loss of p53 has been shown in cultured mouse cells (Fukasawa et al. 1996), but not in cultured human cells (Kawamura et al. 2004). However, loss of p53 and centrosome amplification has been revealed in human cancer tissue. Our preliminary examination has indicated a weak correlation between centrosome amplification and chromosome number (data not shown). Only 2.4% of UCBTERT-21 cells contained >3 centrosomes per cell, whereas 11.9% of UCB408E6E7TERT-33, 19.1% of UE6E7T-3 and 14.3% of UBE6T-6 cells contained >3 centrosomes per cell. Thus, further study is still needed to clarify the mechanism inducing chromosomal instability in immortalized hMSCs cultured over a long period.

Human mesenchymal stem cells are thought to be multipotent cells that can replicate stem cells and that can differentiate to lineages of mesenchymal tissues including bone, fat, tendon, and muscle. Our results indicated that immortalized hMSCs, except UCBTERT-21, induced changes in chromosome number over prolonged culture, but these cells have still retained the ability to both proliferate and differentiate. Immortalized UBE6T-6 cells also displayed neuron-like morphology and strong expression of the neuron-specific markers of neurofilament and III-β-tubulin. We previously demonstrated that hTERT, E7-immortalized hMSCs differentiate into neural cells in vitro on the basis of morphological changes, expression of neural markers such as nestin, neurofilament, MAP-2, Nurr1, and III-β-tubulin. Furthermore, the physiological function showed reversible calcium uptake in response to extracellular potassium concentration (Mori et al. 2005). Similar observations have been reported using rat MSCs (Wislet-Gendebien et al. 2003; Wislet-Gendebien et al. 2005; Pacary et al. 2006). In preliminary experiment of cell transplantation that 10^6 cells of UCBTERT-21 cell (PDLs 120) or UCB408E6E7TERT-33 cell (PDLs 200) were injected into nude mice subcutaneously, no tumorigenicity was observed (data not shown).

In conclusion, our study showed that the hTERT-immortalized cell line displayed normal karyotype and differentiation ability in prolonged culture. These results provide a step forward toward supplying a sufficient number of cells for new therapeutic approaches. In addition, oncogene-immortalized cell lines exhibited abnormal karyotype accompanying the preferential loss of chromosome 13 but without differential alteration during prolonged culture. Thus, the results could provide a useful model for understanding the mechanisms of the chromosomal instability and the differentiation of hMSC.

Acknowledgments This study was supported in part by a grant from the Ministry of Health, Labor and Welfare of Japan. We are grateful to Dr. T.Masui for his advice on ethics problems, and to Mr. H.Migitaka (Carl Zeiss Co., Ltd.) for his assistance with mFISH karyotype analysis. M.T. and K.T. contributed equally to this work.

References

Armanios, M.; Greider, C. W. Telomerase and cancer stem cells. Cold Spring Harbor Symp. Quant. Biol. 70:205–208; 2005.

Bodnar, A. G.; Ouellette, M.; Frolkis, M.; Holt, S. E.; Chiu, C. P.; Morin, G. B.; Harley, C. B.; Shay, J. W.; Lichtsteiner, S.; Wright, W. E. Extension of life-span by introduction of telomerase into normal human cells. Science 279:349–352; 1998.

Burns, J. S.; Abdallah, B. M.; Guldberg, P.; Rygaard, J.; Schroder, H. D.; Kassem, M. Tumorigenic heterogeneity in cancer stem cells evolved from long-term cultures of telomerase-immortalized human mesenchymal stem cells. Cancer Res. 65:3126–3135; 2005.

Carlson, J. A.; Healy, K.; Tran, T. A.; Malfetano, J.; Wilson, V. L.; Rohwedder, A.; Ross, J. S. Chromosome 17 aneusomy detected by fluorescence in situ hybridization in vulvar squamous cell carcinomas and synchronous vulvar skin. Am. J. Pathol. 157:973–983; 2000.

Chang, M. W.; Grillari, J.; Mayrhofer, C.; Fortschegger, K.; Allmaier, G.; Marzban, G.; Katinger, H.; Voglauer, R. Comparison of early passage, senescent and hTERT immortalized endothelial cells. Exp. Cell Res. 309:121–136; 2005.

Cross, S. M.; Sanchez, C. A.; Morgan, C. A.; Schimke, M. K.; Ramel, S.; Idzerda, R. L.; Raskind, W. H.; Reid, B. J. A p53-dependent mouse spindle checkpoint. Science 267:1353–1356; 1995.

Dickson, M. A.; Hahn, W. C.; Ino, Y.; Ronfard, V.; Wu, J. Y.; Weinberg, R. A.; Louis, D. N.; Li, F. P.; Rheinwald, J. G. Human keratinocytes that express hTERT and also bypass a p16(INK4a)-enforced mechanism that limits life span become immortal yet retain normal growth and differentiation characteristics. Mol. Cell Biol. 20:1436–1447; 2000.

Draper, J. S.; Smith, K.; Gokhale, P.; Moore, H. D.; Maltby, E.; Johnson, J.; Meisner, L.; Zwaka, T. P.; Thomson, J. A.; Andrews, P. W. Recurrent gain of chromosomes 17q and 12 in cultured human embryonic stem cells. Nat. Biotechnol. 22:53–54; 2004.

Duensing, S.; Lee, L. Y.; Duensing, A.; Basile, J.; Piboonniyom, S.; Gonzalez, S.; Crum, C. P.; Munger, K. The human papillomavirus type 16 E6 and E7 oncoproteins cooperate to induce mitotic defects and genomic instability by uncoupling centrosome duplication from the cell division cycle. Proc. Natl. Acad.Sci. U. S. A. 97:10002–10007; 2000.

Duensing, S.; Munger, K. The human papillomavirus type 16 E6 and E7 oncoproteins independently induce numerical and structural chromosome instability. Cancer Res. 62:7075–7082; 2002.

Fukasawa, K.; Choi, T.; Kuriyama, R.; Rulong, S.; Vande Woude, G. F. Abnormal centrosome amplification in the absence of p53. Science 271:1744–1747; 1996.

Harada, H.; Nakagawa, H.; Oyama, K.; Takaoka, M.; Andl, C. D.; Jacobmeier, B.; von, W. A.; Enders, G. H.; Opitz, O. G.; Rustgi, A. K. Telomerase induces immortalization of human esophageal keratinocytes without p16INK4a inactivation. Mol. Cancer Res. 1:729–738; 2003.

Kawamura, K.; Izumi, H.; Ma, Z.; Ikeda, R.; Moriyama, M.; Tanaka, T.; Nojima, T.; Levin, L. S.; Fujikawa-Yamamoto, K.; Suzuki, K.; Fukasawa, K. Induction of centrosome amplification and

chromosome instability in human bladder cancer cells by p53 mutation and cyclin E overexpression. Cancer Res. 64:4800–4809; 2004.

Khan, S. H.; Wahl, G. M. p53 and pRb prevent rereplication in response to microtubule inhibitors by mediating a reversible G1 arrest. Cancer Res. 58:396–401; 1998.

Kiyono, T.; Foster, S. A.; Koop, J. I.; McDougall, J. K.; Galloway, D. A.; Klingelhutz, A. J. Both Rb/p16INK4a inactivation and telomerase activity are required to immortalize human epithelial cells. Nature 396:84–88; 1998.

Makino, S.; Fukuda, K.; Miyoshi, S.; Konishi, F.; Kodama, H.; Pan, J.; Sano, M.; Takahashi, T.; Hori, S.; Abe, H.; Hata, J.; Umezawa, A.; Ogawa, S. Cardiomyocytes can be generated from marrow stromal cells in vitro. J. Clin. Invest. 103:697–705; 1999.

Milyavsky, M.; Shats, I.; Erez, N.; Tang, X.; Senderovich, S.; Meerson, A.; Tabach, Y.; Goldfinger, N.; Ginsberg, D.; Harris, C. C.; Rotter, V. Prolonged culture of telomerase-immortalized human fibroblasts leads to a premalignant phenotype. Cancer Res. 63:7147–7157; 2003.

Mori, T.; Kiyono, T.; Imabayashi, H.; Takeda, Y.; Tsuchiya, K.; Miyoshi, S.; Makino, H.; Matsumoto, K.; Saito, H.; Ogawa, S.; Sakamoto, M.; Hata, J.; Umezawa, A. Combination of hTERT and bmi-1, E6, or E7 induces prolongation of the life span of bone marrow stromal cells from an elderly donor without affecting their neurogenic potential. Mol. Cell Biol. 25:5183–5195; 2005.

Munger, K.; Baldwin, A.; Edwards, K. M.; Hayakawa, H.; Nguyen, C. L.; Owens, M.; Grace, M.; Huh, K. Mechanisms of human papillomavirus-induced oncogenesis. J. Virol. 78:11451–11460; 2004.

Munger, K.; Howley, P. M. Human papillomavirus immortalization and transformation functions. Virus Res. 89:213–228; 2002.

Okamoto, T.; Aoyama, T.; Nakayama, T.; Nakamata, T.; Hosaka, T.; Nishijo, K.; Nakamura, T.; Kiyono, T.; Toguchida, J. Clonal heterogeneity in differentiation potential of immortalized human mesenchymal stem cells3. Biochem. Biophys. Res. Commun. 295:354–361; 2002.

Olaharski, A. J.; Sotelo, R.; Solorza-Luna, G.; Gonsebatt, M. E.; Guzman, P.; Mohar, A.; Eastmond, D. A. Tetraploidy and chromosomal instability are early events during cervical carcinogenesis. Carcinogenesis 27:337–343; 2006.

Pacary, E.; Legros, H.; Valable, S.; Duchatelle, P.; Lecocq, M.; Petit, E.; Nicole, O.; Bernaudin, M. Synergistic effects of CoCl(2) and ROCK inhibition on mesenchymal stem cell differentiation into neuron-like cells. J. Cell Sci. 119:2667–2678; 2006.

Patel, D.; Incassati, A.; Wang, N.; McCance, D. J. Human papillomavirus type 16 E6 and E7 cause polyploidy in human keratinocytes and up-regulation of G2-M-phase proteins. Cancer Res. 64:1299–1306; 2004.

Pittenger, M. F.; Mackay, A. M.; Beck, S. C.; Jaiswal, R. K.; Douglas, R.; Mosca, J. D.; Moorman, M. A.; Simonetti, D. W.; Craig, S.; Marshak, D. R. Multilineage potential of adult human mesenchymal stem cells. Science 284:143–147; 1999.

Saito, M.; Handa, K.; Kiyono, T.; Hattori, S.; Yokoi, T.; Tsubakimoto, T.; Harada, H.; Noguchi, T.; Toyoda, M.; Sato, S.; Teranaka, T. Immortalization of cementoblast progenitor cells with Bmi-1 and TERT. J. Bone Miner. Res. 20:50–57; 2005.

Schaeffer, A. J.; Nguyen, M.; Liem, A.; Lee, D.; Montagna, C.; Lambert, P. F.; Ried, T.; Difilippantonio, M. J. E6 and E7 oncoproteins induce distinct patterns of chromosomal aneuploidy in skin tumors from transgenic mice. Cancer Res. 64:538–546; 2004.

Sen, S. Aneuploidy and cancer. Curr. Opin. Oncol. 12:82–88; 2000.

Shi, Q.; King, R. W. Chromosome nondisjunction yields tetraploid rather than aneuploid cells in human cell lines. Nature 437:1038–1042; 2005.

Solinas-Toldo, S.; Durst, M.; Lichter, P. Specific chromosomal imbalances in human papillomavirus-transfected cells during progression toward immortality. Proc. Natl. Acad. Sci. U. S. A. 94:3854–3859; 1997.

Takeda, Y.; Mori, T.; Imabayashi, H.; Kiyono, T.; Gojo, S.; Miyoshi, S.; Hida, N.; Ita, M.; Segawa, K.; Ogawa, S.; Sakamoto, M.; Nakamura, S.; Umezawa, A. Can the life span of human marrow stromal cells be prolonged by bmi-1, E6, E7, and/or telomerase without affecting cardiomyogenic differentiation? J. Gene Med. 6:833–845; 2004.

Takeuchi, K.; Kuroda, K.; Ishigami, M.; Nakamura, T. Actin cytoskeleton of resting bovine platelets. Exp. Cell Res. 186:374–380; 1990.

Terai, M.; Uyama, T.; Sugiki, T.; Li, X. K.; Umezawa, A.; Kiyono, T. Immortalization of human fetal cells: the life span of umbilical cord blood-derived cells can be prolonged without manipulating p16INK4a/RB braking pathway. Mol. Biol. Cell 16:1491–1499; 2005.

Wislet-Gendebien, S.; Hans, G.; Leprince, P.; Rigo, J. M.; Moonen, G.; Rogister, B. Plasticity of cultured mesenchymal stem cells: switch from nestin-positive to excitable neuron-like phenotype. Stem Cells 23:392–402; 2005.

Wislet-Gendebien, S.; Leprince, P.; Moonen, G.; Rogister, B. Regulation of neural markers nestin and GFAP expression by cultivated bone marrow stromal cells. J. Cell Sci. 116:3295–3302; 2003.

Zheng, L.; Lee, W. H. The retinoblastoma gene: a prototypic and multifunctional tumor suppressor. Exp. Cell Res. 264:2–18; 2001

In Vitro Cell.Dev.Biol.—Animal (2007) 43:168–175
DOI 10.1007/s11626-007-9033-5

Species identification of animal cells by nested PCR targeted to mitochondrial DNA

Kazumi Ono · Motonobu Satoh · Touho Yoshida · Yutaka Ozawa · Arihiro Kohara · Masao Takeuchi · Hiroshi Mizusawa · Hidekazu Sawada

Received: 5 March 2007 / Accepted: 17 April 2007 / Published online: 22 May 2007 / Editor: J. Denry Sato

Abstract We developed a highly sensitive and convenient method of nested polymerase chain reaction (PCR) targeted to mitochondrial deoxyribonucleic acid (DNA) to identify animal species quickly in cultured cells. Fourteen vertebrate species, including human, cynomolgus monkey, African green monkey, mouse, rat, Syrian hamster, Chinese hamster, guinea pig, rabbit, dog, cat, cow, pig, and chicken, could be distinguished from each other by nested PCR. The first PCR amplifies mitochondrial DNA fragments with a universal primer pair complementary to the conserved regions of 14 species, and the second PCR amplifies the DNA fragments with species-specific primer pairs from the first products. The species-specific primer pairs were designed to easily distinguish 14 species from each other under standard agarose gel electrophoresis. We further developed the multiplex PCR using a mixture of seven species-specific primer pairs for two groups of animals. One was comprised of human, mouse, rat, cat, pig, cow, and rabbit, and the other was comprised of African green monkey, cynomolgus monkey, Syrian hamster, Chinese hamster, guinea pig, dog, and chicken. The sensitivity of the PCR assay was at least 100 pg DNA/reaction, which was sufficient for the detection of each species of DNA. Furthermore, the nested PCR method was able to identify the species in the interspecies mixture of DNA. Thus, the method developed in this study will provide a useful tool for the authentication of animal species.

Keywords Cell line authentication · Cross-contamination · Quality control · Bio-resources

K. Ono · M. Satoh (✉) · T. Yoshida · H. Sawada
Health Science Research Resources Bank (HSRRB),
Japan Health Sciences Foundation,
2-11-Rinku-minamihama, Sennan-shi,
Osaka 590-0535, Japan
e-mail: hsrrb@osa.jhsf.or.jp

Y. Ozawa · A. Kohara · M. Takeuchi · H. Mizusawa
Japanese Collection of Research Bioresources (JCRB),
Division of Bioresources,
National Institute of Biomedical Innovation,
7-6-8 Saito-Asagi, Ibaraki-shi,
Osaka 567-0085, Japan

Introduction

It has been occasionally reported that cell lines derived from a certain source can be contaminated with another cell line. This cross-culture contamination is a serious problem for investigations using culture cells (Nelson-Rees et al. 1981). Therefore, it is very important to confirm the identities of cell lines as part of quality control in the operation of the cell banks that supply these cells to researchers. Some methods have been developed for the authentication of cell lines. For example, short tandem repeat profiling has been used to identify human-origin cell lines (Tanabe et al. 1999; Masters et al. 2001). As for the methods to detect interspecies cross-contamination, chromosome typing, immunological testing, and isoenzyme analysis have been used (Montes de Oca et al. 1969; Stulberg 1973; Doyle et al. 1990). Each of these methods, however, has disadvantages, such as chromosome analysis, which requires great skill, and immunological identification, which requires species-specific antibodies. Isoenzyme analysis is a general method to find

interspecies cross-contamination (Steube et al. 1995). However, the sensitivity of this technique is not suitable for the detection of intermingling with other species-derived cells (Nims et al. 1998), and some specialized reagents and devices are required.

The identification of species by polymerase chain reaction (PCR) based on species-specific deoxyribonucleic acid (DNA) sequences has many advantages, as follows: (1) the equipment required for PCR has become widespread in the laboratories of life science research, (2) the method is relatively simple and does not require great skill, and (3) the sensitivity is high because of amplification of a specific DNA fragment. Thus, some PCR methods for identification of animal species, including cell line authentication, have been reported in recent years (Naito et al. 1992; Hershfield et al. 1994; Parodi et al. 2002; Liu et al. 2003; Steube et al. 2003). However, these methods are not suitable for the purpose of rapidly distinguishing many kinds of animal species.

In the present study, we developed a highly sensitive PCR method that can distinguish 14 animal species, which are commonly used in cell cultures for life science research; i.e., human, cynomolgus monkey, African green monkey, mouse, rat, Syrian hamster, Chinese hamster, guinea pig, rabbit, dog, cat, cow, pig, and chicken.

Materials and Methods

Cell lines and preparation of DNA. All cell lines used in this study are shown in Table 1 and are available from the Health Science Research Resources Bank (HSRRB). These cell lines were confirmed to be free of microorganisms, such as mycoplasma, bacteria, fungi and yeast, and the species in the original description was authenticated by isoenzyme analysis at the HSRRB. Cellular DNA containing both nuclear and mitochondrial DNA was extracted using MagExtractor-Genome (Toyobo. Co., Ltd., Osaka, Japan) according to the manufacturer's instruction, and the resultant purified DNA was used for PCR.

Primer design. The information of full-length and partial mitochondrial DNA sequences for 14 species of animals were obtained from the published database at the National Center for Biotechnology Information (NCBI). The accession numbers of the reference sequences and the area corresponding to each primer's target are listed in Table 2, and the nucleotide sequences of each primer are presented in Table 3. The first primers, which were complementary to conserved sequences within cytochrome *b* (for forward primer) and 16S ribosomal RNA genes (for reverse) among the 14 species, were designed as a universal primer pair (Fig. 1). The amplified product covers cytochrome *b*, d-loop, 12S ribosomal RNA and 16S ribosomal RNA genes, and the predicted product size is 4–5 kbp. The species-specific sequences within the area amplified by the universal primer pair were selected as second primer pairs. To clearly identify the species-specific bands in agarose gel electrophoresis, we designed 2nd primers for the 14 species to amplify different sizes of DNA in the range of 200–1400 bp at approximately 50-bp intervals (Table 2; see also Fig. 3*A*).

Polymerase chain reaction. The 50-μl reaction mixture contained 1.25 units Takara Ex Taq (Takara Bio, Inc., Otsu, Japan), Ex Taq buffer (Mg^{2+}: 2 mM), dNTPs (50 μM each), 10 pmol of each primer and 100 ng of sample DNA, unless otherwise stated. The amplification was carried out in a PCR Thermal Cycler MP (TP3000; Takara Bio Inc.). In the first PCR, the reaction mixture was heated at 94° C for 5 min, at 59° C for 5 min, followed by 35 cycles of elongation at 72° C for 2.5 min, denaturation at 94° C for 30 s, annealing at 59° C for 45 s, with elongation at 72° C

Table 1. Cell lines used in this study

Name of cell line	Registry number	Species
293	JCRB9068	Human
A549	JCRB0076	Human
COLO320 DM	JCRB0225	Human
HuH-7	JCRB0403	Human
HeLa S3	JCRB9010	Human
Hep G2	JCRB1054	Human
JTC-12	JCRB0607	Cynomolgus monkey
MK.P3	JCRB0607.1	Cynomolgus monkey
COS-7	JCRB9127	African green monkey
Vero	JCRB9013	African green monkey
3T3-L1	JCRB9014	Mouse
A9	JCRB0221	Mouse
B16 melanoma	JCRB0202	Mouse
KUM3	JCRB1134	Mouse
WEHI-3b	IFO50296	Mouse
C6	IFO50110	Rat
L6	JCRB9081	Rat
Py-3Y1-S2	JCRB0736	Rat
WB-F344	JCRB0193	Rat
BHK(C-13)	JCRB9020	Syrian hamster
RPMI 1846	JCRB9087	Syrian hamster
CHO-K1	IFO50414	Chinese hamster
TG-1	JCRB0626	Chinese hamster
104C1	JCRB9036	Guinea pig
SIRC	IFO50020	Rabbit
MDCK	IFO50071	Dog
CRFK	JCRB9035	Cat
PG4(S+L−)	JCRB9125	Cat
MDBK	JCRB9028	Cow
PK(15)	JCRB9030	Pig
DT40	JCRB9130	Chicken
LMH	JCRB0237	Chicken
4G12 hybridoma	IFO50090	Hybrid (human × mouse)
N18-RE-105	IFO50221	Hybrid (mouse × rat)

Table 2. The target sequence position for each primer pair in the mitochondrial genome and the predicted size of the amplified product

Species	Primer						Reference mitochondrial DNA sequence (NCBI accession number)
	First primer		Second primer				
	Forward	Reverse	Forward	Reverse	Genes amplified	Predicted product size (bp)	
Human	15226–15249	2990–3009	15311–15334	15732–15751	Cyt b	441	NC 001807
Cynomolgus monkey	479–502[(a)]	1572–1591[(b)]	209–229[(c)]	1320–1340[(c)]	12S→16S	1132	(a)AF295584, (b)AF420036, (c)AF424970
African green monkey	14643–14666	2408–2427	800–823	1074–1100	12S→16S	301	AY863426.1
Mouse	14623–14646	2430–2449	28–55	954–975	tRNA-Phe→12S	948	NC 005089
Rat	14602–14625	2419–2438	1748–1767	2218–2240	16S	493	NC 001665
Syrian hamster	479–502	ND[a]	682–703	906–926	Cyt b	245	AF119265
Chinese hamster	14604–14627	2413–2432	353–376	930–953	12S	601	DQ390542
Guinea pig	14642–14665	2494–2413	140–159	454–478	12S	339	NC 000884
Rabbit	14653–14676	2425–2444	116–136	799–819	12S	704	NC 001913
Dog	14668–14691	2428–2447	1105–1125	1838–1859	16S	755	AY729880
Cat	15516–15539	3288–3307	1675–1694	3046–3065	12S→16S	1391	NC 001700
Cow	14991–15014	2781–2800	401–421	1469–1490	tRNA-Phe→16S	1090	AB074965
Pig	15791–15814	3568–3587	2099–2123	2898–2917	12S→16S	819	AY337045
Chicken	15383–15406	3715–3734	3395–3415	3570–3591	16S	197	AB086102

Cyt b cytochrome b, *tRNA-Phe* phenylalanine transfer RNA, *12S* 12S ribosomal RNA, and *16S* 16S ribosomal RNA
[a] The corresponding 16S ribosomal RNA genome sequence of Syrian hamster was not available.
[(a)] means reference sequence AF295584.
[(b)] means reference sequence AF420036.
[(c)] means reference sequence AF424970.

for 10 min in the last cycle, and stored at 4° C. The first amplified product was diluted to 1:10 with sterile distilled water, and a 1 μl aliquot of the diluted product was used as the sample DNA for the second PCR. In the second PCR, the reaction mixture was heated to 94° C for 5 min, maintained at 60° C for 5 min, followed by 30 cycles of elongation at 72° C for 1.5 min, denaturation at 94° C for 45 s, annealing at 60° C for 30 s, with elongation at 72° C for 10 min in the last cycle, and stored at 4° C. Each 5 μl of second PCR product was run on a 2% agarose (SeaKem GTG agarose; Cambrex Bio Science Rockland, Inc., Rockland, ME) minigel unless otherwise noted, stained

Table 3. Nucleotide sequences of each primer pair

Primer pair	Forward sequence	Reverse sequence
First PCR primer	THGTHSAATGAATCTGAGGVGGVT	CGATGTTGGATCAGGACATC
Second PCR primer		
Human	TATTGCAGCCCTAGCAGCACTCCA	AGAATGAGGAGGTCTGCGGC
Cynomolgus monkey	AGTGAGCGCAAACGCCACTGC	GTTAACAGTGAAGGTGGCATG
African green monkey	CCAGAAGACCCACGATAACTCTCA	TGTTAGCTCAAGGTAATCGAGTTGTAC
Mouse	GCACTGAAAATGCTTAGATGGATAATTG	CCTCTCATAAACGGATGTCTAG
Rat	CAATCCACCAAGCACAAGTG	CCCCAACCGAAATTTGGTAGTTC
Syrian hamster	GACCTCTTAGGTGTATTCCTAC	GTATGAAGAAGGGGTAGAGCA
Chinese hamster	CCGGCGTAAAACGTGTTATAGACT	GTATTAGGTATAATATCGGCAGTC
Guinea pig	GCCCTATGTACCACACTCAG	CCTTAGCTTTCGTGTGTCGGACTTA
Rabbit	CATGCAAGACTCCTCACGCCA	GGGCTTTCGTATATTCTGAAG
Dog	GCCCAACTAACCCCAAACTTA	GGTTAACAATGGGGTGGATAAG
Cat	TAGAACACCCACGAAGATCC	CATATGGTCTCTTTGGGTCG
Cow	CCTAGATGAGTCTCCCAACTC	GTTGTTTAGTCGAGAGGGTATC
Pig	CCTATATTCAATTACACAACCATGC	GCGTGTGCGAGGAGAAAGGC
Chicken	GTATTCCCGTGCAAAAACGAG	CTTAGTGAAGAGTTGTGGTCTG

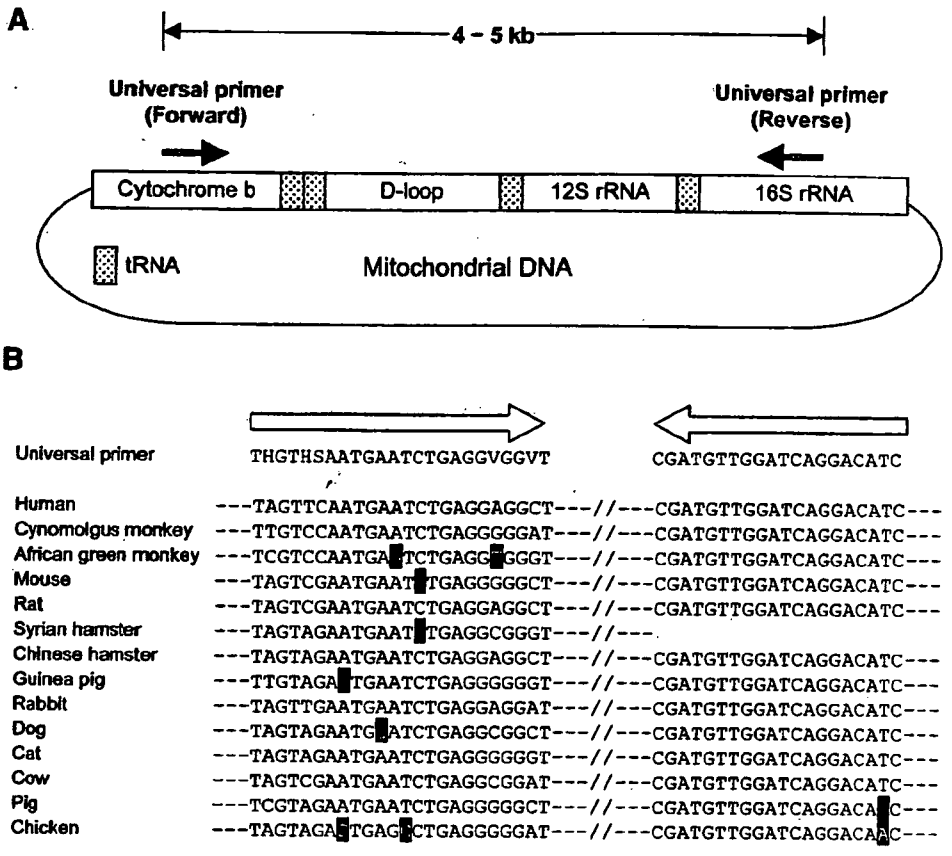

Figure 1. Universal primer pairs for the first PCR. (*A*) The target position in the mitochondrial DNA. The first PCR is expected to amplify 4- to 5-kb DNA fragments spanning from cytochrome *b* to 16S rRNA. (*B*) The sequences of the universal primers and the target nucleotide of 14 animal species. The forward primer was designed to be complementary to the conserved sequences within cytochrome *b* and the reverse primer within 16S ribosomal RNA, respectively. Degenerate primer was used for the forward primer, i.e., H;A/C/T, S;C/G, V;A/C/G. Inversed letters indicate bases mismatched to universal primer sequences. The 16S rRNA sequence of Syrian hamster for reverse primer was not available from the NCBI database.

with ethidium bromide, visualized under UV light (Mupid-Scope WD; Advance Co., Ltd., Tokyo, Japan), and photographed. The 100 bp DNA Ladder (Takara Bio Inc.) was applied as a size marker.

Result and Discussion

First PCR. Mitochondrial DNA is generally a desirable target for PCR compared with nuclear DNA, as each animal cell generally contains 500–1,000 copies of mitochondrial DNA. Primers were designed as described in "Materials and Methods". Figure 2 shows the gel electrophoresis of the first PCR products amplified with the universal primer pair from each species DNA. The predicted 4- to 5-kbp products were clearly observed for all species, except for chicken. In the case of chicken, no visible band was observed at ca. 5 kbp, the size predicted from chicken mitochondrial DNA sequence. However, it is likely that specific amplification does occur during the first PCR for chicken DNA, because a much larger amount of chicken DNA was required without first PCR for identification during the second PCR compared with that obtained when first PCR was carried out (data not shown).

Species-specificity of nested PCR. The nested PCR strategy was used to specifically amplify species-specific DNA. To confirm amplification by each species-specific primer pair, DNA prepared from each cell line originating from 14 species of animals was subjected to the nested PCR using the universal primer pair in the first PCR and the respective single species-specific primer pair in the second PCR. The amplified product from the corresponding species DNA exhibited the predicted size (Table 2) for each animal species, and could be readily distinguished from each other according to the different sizes (Fig. 3*A*). Figure 3*B* shows the species-specificity of nested PCR in this strategy. Most of the species-specific primer pairs, i.e., human, cynomolgus monkey, Syrian hamster, Chinese ham-

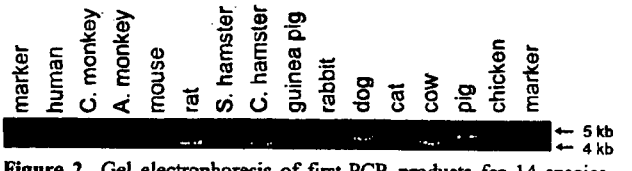

Figure 2. Gel electrophoresis of first-PCR products for 14 species. DNA of each species was extracted from the following cell lines indicated in *parentheses*, human (A549), cynomolgus monkey (MK.P3), African green monkey (COS-7), mouse (WEHI-3b), rat (Py-3Y1-S2), Syrian hamster (BHK-1 (C-13)), Chinese hamster (CHO-K1), guinea pig (104C1), rabbit (SIRC), dog (MDCK), cat (PG-4(S+L−)), cow (MDBK), pig (PK15), chicken (LMH) for amplification using the universal primer pair. The amplified DNA fragments were run on a 1% agarose gel.

ster, guinea pig, dog, cat, cow, pig, and chicken primers, amplified the specific DNA only from the corresponding species DNA. In the PCR using primer pairs specific for rabbit and African green monkey, however, unexpected bands appeared in addition to the predicted ones. The rabbit primer pair amplified cynomolgus monkey DNA, but the product could be readily distinguished from the rabbit-specific band because of their different sizes. The primer pair for African green monkey also produced an approximately 300-bp-sized band for cynomolgus monkey DNA, which was similar in size

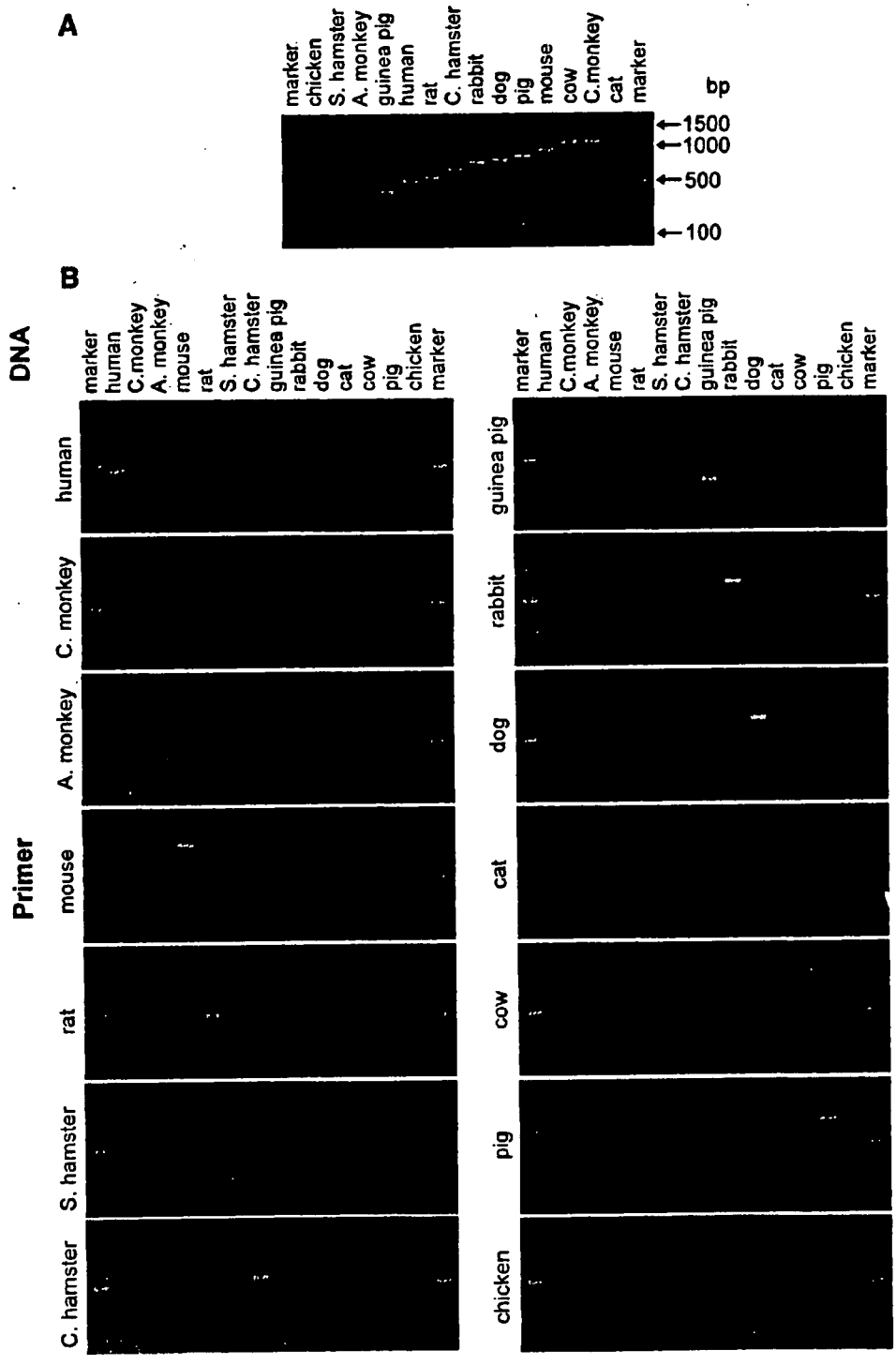

Figure 3. Gel electrophoresis of the second-PCR products for 14 species. The same cell lines as in Fig. 2 were used. (*A*) DNA of each species was subjected to nested PCR using corresponding species-specific primer pairs in the second PCR. The second-PCR products were aligned in size-order as a ladder. The amplification products were distinguished by the size. (*B*) Species specificity of the nested PCR. The 14 species-derived DNA was amplified with the universal primer pair and further amplified with the second primer pair indicated on the left side of each photograph.